

stretching of the macromolecules is dominated by the extensional component of the flow; the influence of the shearing component is negligible unless the extensional component is almost entirely absent.

3.6.2.2 Simple Theories

3.6.2.2.1 FINITE EXTENSIBILITY. The rheological data for dilute solutions described above (in Section 3.6.2.1) indicate that the main limitation of the Hookean dumbbell (or the Oldroyd-B) model is that it assumes that the polymer molecules are infinitely extensible, which is objectionable for large molecular extensions. Fortunately, this defect of the elastic dumbbell model can be corrected simply by making the relation between the spring force, \mathbf{F}^s , and the molecular extension, \mathbf{R} , nonlinear, such that the force becomes very large as the molecular extension approaches the fully extended length L of the molecule. For example, for a *freely jointed chain* with many bonds (see Section 2.2.3.2), the force–extension relationship is an *inverse Langevin function*. The Langevin function is defined in Eq. (8-28); its inverse is not an analytic form, but it can be roughly approximated by the analytic *Warner spring law* (Warner 1972), also known as the “FENE” (finitely extensible, nonlinear-elastic) spring:

$$\mathbf{F}^s = \frac{2\beta^2 k_B T}{1 - (R/L)^2} \mathbf{R} \equiv H(R^2) \mathbf{R} \quad (3-56)$$

where $H \equiv 2\beta^2 k_B T / (1 - (R/L)^2)$ is the nonlinear spring coefficient. Also, $\beta^2 \equiv 3 / (2N_K b_K^2)$, and $L = N_K b_K$. N_K is the number of links in the freely jointed chain, and b_K is the length of each link. Figure 3-18 compares the force law for the Warner spring with those for the inverse Langevin function and the linear Hookean spring. Significant departures ($\sim 10\%$) from linear behavior occur when the chain reaches a third of its full extension, and these deviations become large ($> 30\%$) when it exceeds half of its full extension. The inverse Langevin function and the Warner spring law are appropriate for most synthetic polymers whose flexibility can be approximated by the freely jointed chain model (see Section 2.2.3.2).

The freely jointed chain model is most appropriate for synthetic polymers, such as polyethylene and polystyrene. For other molecules, such as DNA and polypeptides, the molecular flexibility is better described by the *worm-like chain model* (described in Section 2.2.4), whose force law can be approximated by a simple expression due to Marko and Siggia (1995), namely,

$$\frac{F^s \lambda_p}{k_B T} = \frac{1}{4} \left(1 - \frac{R}{L}\right)^{-2} - \frac{1}{4} + \frac{R}{L} \quad (3-57)$$

where L is the contour length of the molecule, and λ_p is the persistence length (see Section 2.2.4). This force law has been confirmed by direct measurements on a single DNA molecule attached at one end to a surface and attached at the other end to a magnetic bead and then stretched under magnetic and hydrodynamic fields under a microscope (Smith et al. 1992). [The vector force \mathbf{F}^s can be obtained from the scalar force F^s in Eq. (3-57) by multiplying it by a unit vector parallel to the molecule’s end-to-end vector.] At high extensions, the Marko–Siggia expression approaches a limit somewhat similar to that of the Warner spring: $\mathbf{F}^s \rightarrow (k_B T / 4\lambda_p L)(1 - R/L)^{-2}$.

When a nonlinear spring law is used in the dumbbell model, the Smoluchowski equation (3-28) is changed to

$$\frac{\partial}{\partial t} \psi = -\frac{\partial}{\partial \mathbf{R}} \cdot \left[\mathbf{R} \cdot \nabla \psi - \frac{2k_B T}{\zeta} \left(\frac{1}{k_B T} H(R^2) \mathbf{R} \psi + \frac{\partial \psi}{\partial \mathbf{R}} \right) \right] \quad (3-58)$$

Because $H(R^2)$ is not a constant, an analytic expression for the stress tensor cannot be obtained from Eq. (3-58) unless an approximation is made. A common approximation is to replace $H(R^2)$ by the *preaveraged* quantity, $H(\langle R^2 \rangle)$ (Peterlin 1961; Tanner 1985). In this approximation, H is taken to be independent of R^2 , but dependent on the average of R^2 . This means that Eq. (3-58) becomes a linear equation in \mathbf{R} and thus can be solved rather easily. However, preaveraging can be dangerous if there are large fluctuations about the mean value of the preaveraged quantity. For steady-state flows, preaveraging seems to be an acceptable approximation (Tanner 1985). However, in some transient flows, the errors can be significant (Keunings 1997; Doyle et al. 1998). After making the preaveraging approximation, Eq. (3-58) can be multiplied by $\mathbf{R}\mathbf{R}$ and integrated over configuration space in the usual way, yielding

$$\overset{\nabla}{\mathbf{S}} + \frac{1}{\tau} \left(\frac{\mathbf{S}}{1 - (\text{tr} \mathbf{S})/2L^2} - \beta^{-2} \delta \right) = \mathbf{0} \quad (3-59a)$$

where $\mathbf{S} \equiv 2 \langle \mathbf{R}\mathbf{R} \rangle$, and $\tau = \zeta/8k_B T \beta^2$. Because the spring force law is not linear, the stress tensor is not proportional to $\langle \mathbf{R}\mathbf{R} \rangle$, but from Eq. (3-11) is given by

$$\boldsymbol{\sigma} = \nu k_B T \beta^2 \left(1 - \frac{\text{tr} \mathbf{S}}{2L^2} \right)^{-1} \mathbf{S} \quad (3-59b)$$

Since the nonlinearity in the spring law shows up mostly at high molecular extension, the predictions of the FENE dumbbell model are changed from those of a Hookean dumbbell at high shear rates in shearing flows, and in extensional flows when the extension rate $\dot{\epsilon}$ exceeds the critical value $\dot{\epsilon}_c$ for a coil-stretch transition. In shearing flow at high shear rates, the preaveraged FENE, or “FENE-P” dumbbell model, gives

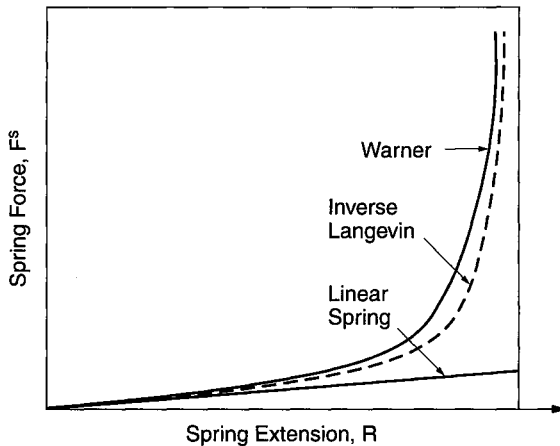


Figure 3.18 Elastic spring force versus molecular extension for the Warner spring, for the freely jointed chain (which is described by the inverse Langevin function), and for the linear spring. (From Tanner, copyright © 1985 by Oxford University Press, Inc. Used by permission of Oxford University Press, Inc.)

$$\frac{\eta_{\infty}^p}{\eta_0} = (\beta L)^{2/3} (\tau \dot{\gamma})^{-2/3}, \quad \frac{\Psi_{1,\infty}}{\Psi_{1,0}} = (\beta L)^{4/3} (\tau \dot{\gamma})^{-4/3} \quad (3-60)$$

For this model, the second normal stress difference is zero at all shear rates. For the freely jointed chain, to which the FENE or FENE-P spring is an approximation, the polymer contribution to the shear viscosity at high shear rates is proportional to $\dot{\gamma}^{-1/2}$, rather than $\dot{\gamma}^{-2/3}$ (Doyle et al. 1997).

For an extensional flow, the polymer contribution to the normal stress difference at high $\dot{\epsilon}$ is

$$\Delta\sigma_p \equiv \sigma_{11,p} - \sigma_{22,p} \sim \nu L F^s(R \rightarrow L) \approx \frac{1}{2} \nu L^2 \zeta \dot{\epsilon}$$

because the spring constant approaches $H \rightarrow \dot{\epsilon} \zeta / 2$ at high $\dot{\epsilon}$ for any finitely extensible spring. The friction coefficient is related to the relaxation time τ by $\zeta = 4H_0\tau$, where $H_0 \equiv 2k_B T \beta^2$ is the spring constant at small extensions. The polymer contribution to the elongational viscosity, $\Delta\sigma_p / \dot{\epsilon}$, at high $\dot{\epsilon}$ therefore approaches a constant:

$$\bar{\eta}_p \rightarrow \bar{\eta}_{p,\infty} = \frac{1}{2} \nu L^2 \zeta = 2\nu L^2 H_0 \tau = 2\nu k_B T B \tau = 2B \eta_{p,0} \quad (3-61)$$

where B is defined as $B \equiv 2\beta^2 L^2$, and $\eta_{p,0}$ is the polymer contribution to the zero-shear viscosity. Since $\beta^2 = 3/(2\langle R^2 \rangle_0)$, the parameter B is three times the square of the ratio of the polymer's fully extended length to its root-mean-square end-to-end separation; that is, $B = 3L^2 / \langle R^2 \rangle_0$. The same asymptotic result is obtained with the Marko-Siggia force law. The fully extended length of a synthetic organic flexible polymer can be estimated as $L \approx 0.82n\ell$, where n is the number of carbon-carbon bonds in the backbone, and $\ell = 1.54\text{\AA}$ is the length of a backbone bond (Flory 1969). The equilibrium mean-square end-to-end separation $\langle R^2 \rangle_0$ in a theta solvent is given by $C_{\infty} n \ell^2$. For good solvents, $\langle R^2 \rangle_0$

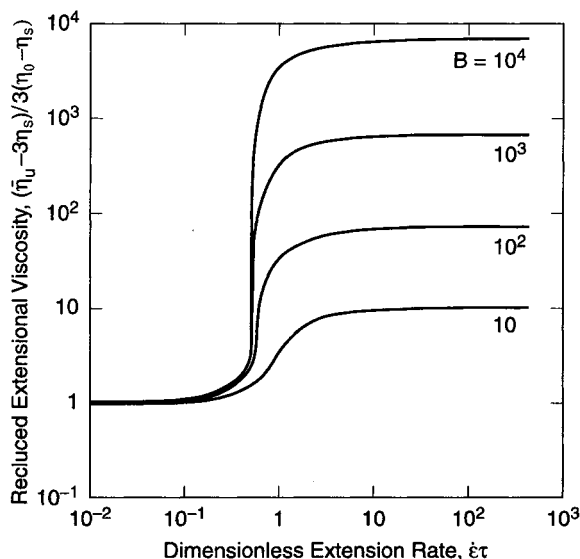


Figure 3.19 The polymer contribution to the steady-state uniaxial extensional viscosity $\bar{\eta}_u$ divided by the polymer contribution to the zero-shear viscosity $\eta_{p,0} = \eta_0 - \eta_s$ for the dumbbell model with a nonlinear “FENE” spring and various values of $B \equiv 2\beta L^2$. (From Bird et al. *Dynamics of Polymeric Liquids, Vol. 2*, Copyright © 1987. Reprinted by permission of John Wiley & Sons, Inc.)

is larger than this, and thus for a given molecular weight, $B \equiv 3L^2/\langle R^2 \rangle_0$ is smaller and the polymer is less “extensible.” The reverse is true in solvents poorer than theta. Figure 3-19 shows the dependence of the steady-state uniaxial extensional viscosity $\bar{\eta}_u$ on $\dot{\epsilon}$ for the Warner dumbbell for various values of B .

Comparisons of the predictions of the FENE dumbbell model with measurements of the extensional viscosity of “dilute” solutions have been fairly encouraging. Figure 3-2 compares the Trouton ratio predicted by a multimode FENE dumbbell model with experimental data for a Boger fluid. Good agreement is obtained if one uses a value of the parameter $B = 3L^2/\langle R^2 \rangle_0 = 40,000$, about a factor of two higher than the estimate from molecular parameters, $B = 20,000$. The discrepancy between the best-fit value of B and the estimate from molecular parameters might be caused by “conformation-dependent drag,” discussed in Section 3.6.2.2.2 below.

Direct observations have recently been made of long ($\sim 20 \mu\text{m}$) DNA molecules undergoing planar extensional flow in a cross-slot apparatus (Perkins et al. 1997). At steady state the degree of extension of the molecules as a function of extension rate agrees with the dumbbell model with a nonlinear worm-like chain spring law. When a molecule is suddenly exposed to an extensional flow with rate modestly above the critical rate for a “coil-stretch” transition, it often first forms a taut section in its middle; the extended portion grows by drawing portions of the chain out of the still-coiled portions attached at each end. This picture of chain unraveling is qualitatively similar to the so-called “yo-yo” model proposed by Ryskin (1987). However, other modes of stretching also occur, including the flattening of the molecule into a “folded” state (Acierno et al. 1974) that is much slower to unravel than the “yo-yo.” Folds are predicted to become prevalent at high Deborah number ($De \gtrsim 10$) (Larson 1990, 1998; Hinch 1994).

3.6.2.2.2 CONFORMATION-DEPENDENT DRAG COEFFICIENT. In the expressions (3-60) and (3-61) for the shear or extensional viscosities at high shear or extension rates, the relaxation time τ was taken to be independent of the average molecular conformation. The success of the Zimm model (Section 3.6.1.2) shows that the polymer relaxations in dilute solutions are dominated by hydrodynamic interactions between different segments on the chain, and one expects these interactions to change when the chain is extended in the flow. Thus, one might expect the effective drag coefficient, and hence the relaxation time, to increase significantly when the molecule is stretched out in a flow field. A simple model for such a change in hydrodynamic drag and relaxation is the *cylinder model* proposed by de Gennes (1974) and Hinch (1974). This model is really just an extension of the “hard sphere” model for the drag on a coiled-up polymer molecule. Recall from Section 3.6.1.1 that the hydrodynamic drag coefficient ζ_{coil} for drag on an unextended polymer coil is proportional to its radius of gyration, which, in turn, scales with molecular length L as L^ν , with $\nu = 0.5$ in a theta solvent. When the molecule is fully extended, the translational drag coefficient ζ_{rod} should be similar to that of a thin cylindrical rod of length L (Doi and Edwards 1986):

$$\zeta_{\text{rod}} = \frac{2\pi L\eta_s}{\ln(L/d)} = \frac{6.28L\eta_s}{\ln(L/d)} \quad (3-62)$$

where d is the molecular diameter.

Since $\zeta_{\text{coil}} \propto L^\nu$ and $\zeta_{\text{rod}} \propto L$, the drag coefficient in the stretched state is very much larger than that in the coiled state *in the limit of high molecular weight*. This

latter qualification is a very important one. Note, in particular, the logarithmic factor $\ln(L/d)$ dividing the right side of Eq. (3-62). From Eqns. (3-48) and (3-62), $\zeta_{\text{rod}}/\zeta_{\text{coil}} \approx \sqrt{n/C_{\infty}}/\ln(L/d)$ for a theta solvent, where n is the number of carbon bonds in the backbone. Because the molecular diameter is so small ($\sim 5\text{--}10 \text{ \AA}$) compared to the length L , for a typical polymer such as polystyrene with molecular weight ranging from 10^5 to 10^7 , L/d ranges from 250 to 25,000, and thus $\ln(L/d) \approx 6\text{--}10$. Hence, ζ_{rod} is only a factor of about 2–14 times larger than ζ_{coil} , except for extraordinarily long molecules ($M > 10^7$). In agreement with this estimate, Doyle et al. (1998) find that the best fits of dumbbell models with conformation-dependent drag to extensional flow data for high-molecular-weight ($M \approx 2 \times 10^6$) polystyrene solutions are obtained when $\zeta_{\text{rod}}/\zeta_{\text{coil}} \approx 8$. Also, direct microscopic observations of the stretching of tethered, fluorescing DNA molecules in uniform flows give results consistent with the theoretical estimate, $\zeta_{\text{rod}}/\zeta_{\text{coil}}$ around 2–3, for DNA aspect ratios L/d of 20,000–75,000 (Larson et al. 1997).

More rigorous treatments of conformation-dependent drag support these inferences. For the multiple beads-and-springs model, detailed theories of conformation-dependent hydrodynamic interactions in shear were developed by Fixman (1966), Öttinger (1985, 1986, 1987), Magda et al. (1988), Kishbaugh and McHugh (1990), and others. In these analyses, the nonequilibrium, flow-distorted distribution function is used to preaverage the Oseen tensors, and these preaveraged Oseen tensors, in turn, are used in the computation of the drag on each bead. The distribution function and the average Oseen tensors are determined *self-consistently*.

Figure 3-20 shows the first normal stress coefficient predicted by Kishbaugh and McHugh for flexible polymer chains of various lengths. For $B \equiv 2\beta^2 L^2 = \infty$ —that is, for an infinitely extensible, Hookean, molecule—the theory predicts *shear thickening* at high shear rates, because of the weakening of hydrodynamic interaction (and hence the increase in the effective drag coefficient) that occurs when the chain is greatly extended. Note, however, that this shear thickening occurs only at rather high dimensionless shear rates. Also, for chains of finite length, shear thickening is terminated at the highest shear rates by the onset of shear thinning produced by finite extensibility. Unless the macromolecule is unusually high in molecular weight, such that $B \gtrsim 3 \times 10^4$, the shear thinning produced by finite extensibility occurs at a shear rate low enough to suppress entirely the shear-thickening phenomenon. For polystyrene in a theta solvent, for example, $B = 3 \times 10^4$ corresponds to a molecular weight of around 10^7 ! Hence, dilute solutions of polystyrene will show shear thickening only for very high molecular weights. Consistent with this, the curve of Ψ_1 versus $\dot{\gamma}$ for a dilute polystyrene solution with $M = 2 \times 10^7$ shown in Fig. 3-16 has a weak shear thickening regime over the range of shear rates expected from the theoretical predictions in Fig. 3-20. (The predicted shear-thickening effect in Fig. 3-20 is highly exaggerated because of the expanded scale of the ordinate.) For polystyrene solutions of molecular weight lower than $\sim 10^7$, such as that for Fig. 3-15, this source of shear thickening can be neglected altogether.

Both the experimental shear-viscosity curve (Fig. 3-16) and the theoretical one (Fig. 3-20) also show a region of weak *shear thinning* at low shear rates. This rather minor phenomenon occurs, according to the theory, because the shear-induced changes in hydrodynamic drag that occur with increasing chain deformation are nonmonotonic. Hydrodynamic interaction can account for both shear thinning at low β^* and shear thickening at high β^* because the hydrodynamic interactions of chain segments that are close to each other are

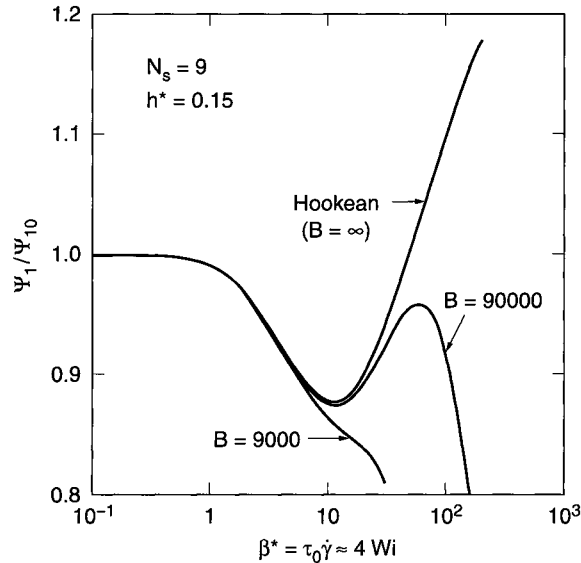


Figure 3.20 Dependence of the first normal stress coefficient on dimensionless shear rate β^* , as predicted by the bead-spring theory with conformation-dependent hydrodynamic interaction and finite extensibility with $N_s = 9$ springs, for various values of B . Here $Wi \equiv \dot{\gamma} \Psi_{1,0} / 2\eta_{p,0}$. (Adapted from J. Non-Newt. Fluid Mech., 34:181, Kishbaugh and McHugh, (1990), with kind permission from Elsevier Science - NL, Sara Burgerhartstraat 25, 1055 KV Amsterdam, The Netherlands.)

qualitatively different from the interactions of segments that are on opposite ends of the chain (Larson 1988). The nonmonotonic effect of hydrodynamic interaction was first pointed out by Peterlin (1960).

In extensional flow, deformation-induced increases in hydrodynamic drag should steepen the coil-stretch transition and, if strong enough, produce hysteresis (de Gennes 1974). These effects can be captured qualitatively by the cylinder model described above. As in the case of shear, these effects are expected to be large in extensional flows only for molecules of high molecular weight (Larson et al. 1997). The interested reader can find further discussion of these issues in Larson (1988) and in articles by de Gennes (1974) and Hinch (1974).

The success of bead-spring models in describing the deformation of flexible polymer molecules is illustrated by some recent comparisons of the predictions of such models against very detailed data for DNA molecules in constant-velocity flows. Figure 3-21 shows the measured and predicted density of DNA mass as a function of position downstream of the point at which the chain is tethered to a small sphere held fixed in position by a laser optical trap (Perkins et al. 1995; Larson et al. 1997). The predictions were obtained without adjustable parameters by using the worm-like chain expression, Eq. (3-57), for the molecular elasticity, the low-shear-rate drag coefficient from diffusivity measurements, Eq. (3-48), and the high-shear-rate drag coefficient from Eq. (3-62). The excellent agreement between theory and experiment for the constant-velocity flow and in planar extensional flows (Larson 1998) indicates that the physics of macromolecular deformation in simple flow fields is well-described by the combination of Brownian motion, a nonlinear elastic spring law, and a weak dependence of the viscous drag coefficient on molecular extension. This inference is supported by recent comparisons of model predictions to extensional flow data for Boger fluids (Doyle et al. 1998). One experimental issue that is as yet unresolved, however, is the failure of light-scattering experiments to show much stretching of polymer

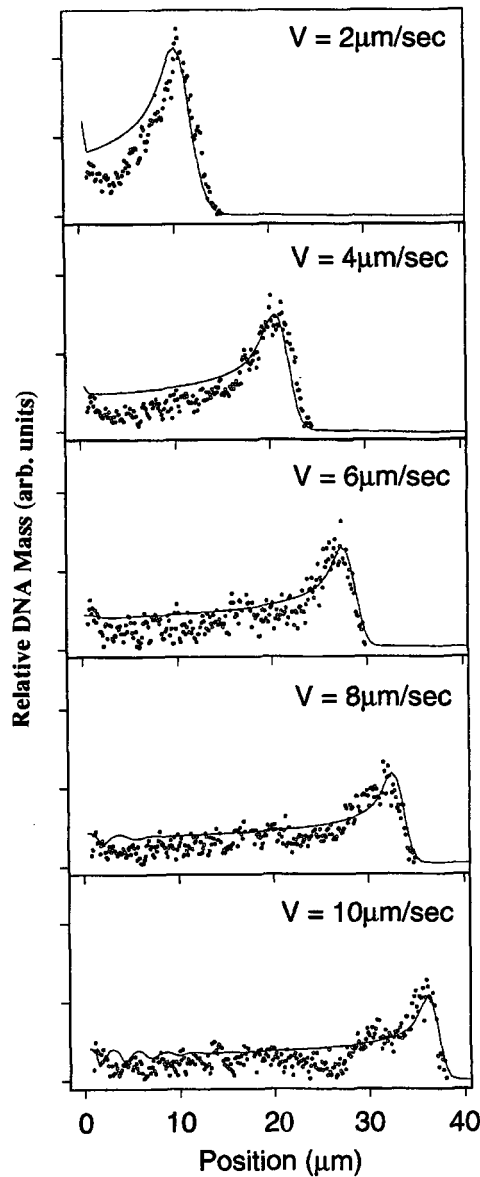


Figure 3.21 Distribution of bead mass as a function of position downstream of the tether point of a DNA molecule of length $L = 67.2 \mu\text{m}$ for various velocities measured in experiments similar to those described in the caption to Fig. 3-1. The lines are the predictions of Monte Carlo molecular simulations using the elastic force from the “worm-like chain” model, Eq. (3-57), and conformation-dependent drag, as described in the text. The value of the parameter $\zeta_{\text{coil}}/k_B T = 4.8 \text{ sec}(\mu\text{m})^{-2}$ is obtained from the diffusivity measurements of Smith et al. (1995); $\zeta_{\text{rod}}/k_B T = 9.1 \text{ sec}(\mu\text{m})^{-2}$ is obtained from Eq. (3-62) for a fully stretched filament. (From Larson et al. 1997, reprinted with permission from the American Physical Society.)

chains, either in shearing flow (Cottrell et al. 1969; Link and Springer 1993; Lee et al. 1997) or even in strong extensional flows (Armstrong et al. 1980; Menasveta and Hoagland 1991).

- Problem 3.6 exercises your ability to compute nonlinear rheological properties of dilute solutions.

3.7 THE RHEOLOGY OF ENTANGLED POLYMERS

In nondilute polymer solutions and melts, the polymer coils interpenetrate each other enough that the molecular motions of one chain are greatly slowed by the interfering effects of other chains. These interferences are attributed to intermolecular *entanglements*.

Despite the complications produced by entanglements, melts and concentrated solutions are free of a couple of complications that exist in dilute solutions. First, in the melt, flexible polymer chains are “ideal”—that is, their configuration distribution is Gaussian. This is because the excluded-volume effect present when the chain is immersed in small-molecule solvent is *screened* by the surrounding chains (Flory 1953; de Gennes 1979). A second complication that appears in dilute solutions but not in melts is *hydrodynamic interaction*. In the melt, experiments show that hydrodynamic interaction is also screened out (Ferry 1980), so that the drag on one part of the chain does not influence the drag on a remote part of the same chain. The great complicating feature of melts is that the motion of each chain is affected by entanglements with the surrounding chains.

The effect of entanglements on the relaxation of polymer chains is illustrated in Fig. 3-22, which shows the storage modulus G' for a series of polystyrene melts of differing

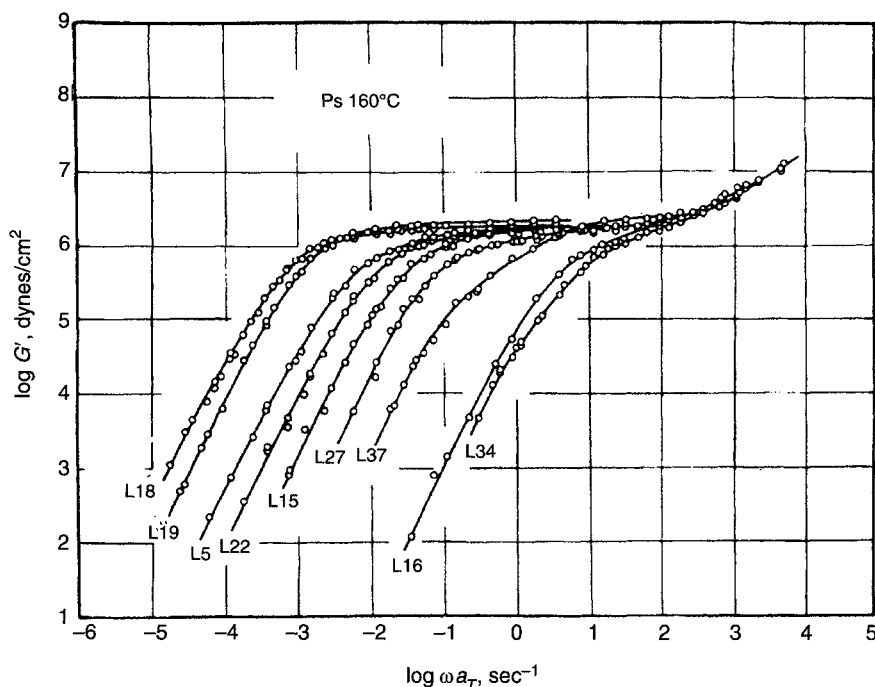


Figure 3.22 Storage modulus, G' , as a function of frequency reduced to 160°C for nearly monodisperse polystyrenes of molecular weight ranging from 580,000 to 47,000, from left to right. (Reprinted with permission from Onogi et al., *Macromolecules* 3:109. Copyright 1970, American Chemical Society.)

molecular weight (Onogi et al. 1970). Notice that there is a *plateau* in G' whose width grows as the molecular weight increases. The plateau value of G' is the *entanglement plateau modulus*, G_N^0 . The molecular weight at which the plateau first appears corresponds roughly to M_c , the molecular weight at which the zero-shear viscosity begins to rise as $M^{3.4}$ (see Fig. 3-3). The terminal, or longest, relaxation time τ_1 of these melts increases with molecular weight with the same power law, $\tau_1 \propto M^{3.4}$. In the frequency range of the plateau, the melt acts like a cross-linked elastic rubber, because G' is nearly constant. The plateau modulus G_N^0 can be related to the density of entanglements, or the density of effective cross-links, ν , by $G_N^0 = (4/5)\nu k_B T$. (The reason for the factor of 4/5 will become apparent in Section 3.7.4.3.) From ν and the bulk density ρ of the polymer, one can obtain the *molecular weight between entanglements*, M_e :

$$M_e = \frac{\rho N_A}{\nu} = \frac{4}{5} \frac{\rho N_A k_B T}{G_N^0} \quad (3-63)$$

It turns out that M_e is about a fifth to a half as large as M_c . The number of monomers between entanglements is denoted $N_e = M_e/M_0$, where M_0 is the molecular weight of a monomer.

The values of M_c and M_e vary from melt to melt; tabulations of these values can be found in Ferry (1980) and Fetters et al. (1994). [Differences in the M_e values between Ferry (1980) and Fetters et al. (1994) are due, in part, to a difference of a factor of 4/5 in the definition of M_e ; here we follow the convention of Fetters et al. (1994).] Some of these M_e values are presented in Table 3-3; the chemical structures of many of these polymers can be found in Fig. 2-7. For highly flexible polymers, M_c usually corresponds to about 300–600 atoms in the backbone of the chain (Ferry 1980); for polystyrene, for example, $M_c \approx 38,000$ and $M_e \approx 13,300$. The magnitude of M_e can be estimated as the minimum molecular weight a chain would need so that the volume of space “pervaded” by the chain is twice that occupied by the chain itself, leaving enough room in the pervaded volume for just one other such chain. This argument suggests that “slender” polymer molecules, which pervade space without themselves taking up much volume, should have lower values of M_e than do “bulky” chains. This suggestion proves indeed to be the case; Fetters et al. (1994) have shown that values of M_e can accurately be predicted from the value of p , a “packing length” that is related to the bulkiness of the molecule (see the end of Section 2.2.3.4):

$$p \equiv \frac{M}{\langle R^2 \rangle_0 \rho N_A} \quad (3-64a)$$

Note that p is independent of molecular weight, since for Gaussian chains $M/\langle R^2 \rangle_0$ is a constant. At 140°C, the entanglement molecular weight M_e , plateau modulus G_N^0 , and the “tube” diameter a (defined below in Section 3.7.1) are related to p by (Fetters et al. 1994)

$$M_e \approx [225.8 \text{ cm}^3 \text{ \AA}^{-3} \text{ mol}^{-1}] p^3 \rho \quad (3-64b)$$

$$G_N^0 \approx [12.16 \text{ MPa \AA}^3] p^{-3} \quad (3-64c)$$

$$a \approx 19.36 p \quad (3-64d)$$

M_e can also be related to K_θ (see Section 3.6.1.1) by

TABLE 3.3
Properties of Polymer Melts

	PE	PS	PDMS	PIB	PMMA	1,4PBd ^a	1,4-PI ^b
Properties at 140°C (from Fetters et al. 1994)							
ρ (g cm ⁻³)	0.784	0.969	0.895	0.849	1.13	0.826	0.830
C_∞	7.3	9.6	6.3	6.8	9.1	5.6	5.0
p (Å)	1.6942	3.9480	4.0593	3.4309	3.4572	2.2946	3.2006
G_N^0 (MPa)	2.60	0.20	0.20	0.32	0.31	1.25	0.42
M_e	828	13,309	12,293	7288	10,013	1815	5429
a (calc.) (Å)	32.8	76.5	78.6	66.4	67.0	44.4	62.0
WLF temperature shift parameters (from Ferry 1980)							
T_g (K)	c	373	150	205	381	205	200
T_0 (K)	c	373	303	298	381	263	248
T_∞ (K)	c	323	81	101	301	149	146
c_1^0	c	12.7	1.90	8.61	34.0	5.97	8.86
c_2^0 (K)	c	50	222	200.4	80	123.2	101.6

PE, polyethylene; PS, polystyrene; PDMS, polydimethylsiloxane; PIB, polyisobutylene; PMMA, (atactic) polymethylmethacrylate; 1,4PBd, 1,4-polybutadiene; 1,4PI, 1,4-polyisoprene.

^aWLF parameters are for "cis-trans-vinyl" polybutadiene from Ferry (1980).

^bWLF parameters are for "Hevea rubber" from Ferry (1980).

^cFor polyethylene, the glass-transition temperature is far below the crystallization temperature; and time-temperature shifting satisfies an Arrhenius form, with activation energy $E_a = 6.5$ kcal/mol for high-density polyethylene.

$$M_e = \left(\frac{\Phi}{B' K_\theta \rho N_A} \right)^2 \quad (3-64e)$$

with $B' = 0.0516$. The above equations give accurate predictions for chains ranging from polyethylene, with $M_e = 830$, to poly(vinylcyclohexane), with $M_e = 39,000$. The coefficients in these equations are somewhat temperature-dependent. The above expressions are similar to those derived by Ronca (1983) and Lin (1987).

3.7.1 Reptation

An explanation for the slowdown of relaxation for melts with $M > M_c$ was given by de Gennes (1971). He considered a simpler problem, that of a single long polymer chain in a cross-linked rubber network, but the results of this analysis can qualitatively be applied to a chain moving in a mesh of other chains (see Fig. 3-23). Since the mesh cannot be crossed, the chain's lateral motion is limited, and the polymer must relax by sliding along its own contour like a snake. De Gennes called this motion *reptation*. The mesh of constraints confines the molecule laterally to a *tube-like* region (Edwards 1967) (see Fig. 3-24). The chain changes its conformation by sliding back and forth along the tube. Those portions of the molecule that escape from the ends of the tube are free to take on random orientations, and the portions of the tube that are vacated are forgotten. By moving back and forth, the chain gradually forgets more and more of the original tube ends; a "new" conformation

diffuses from the ends of the chain inward (see Fig. 3-25). Because it is a diffusive process, the time required for the chain to vacate the original tube is proportional to the square of the *contour length* L_t of the tube divided by the diffusion coefficient of the snaking motion. The diffusion coefficient of the snaking motion is proportional to M^{-1} , while the square of the tube's contour length is proportional to M^2 . Thus the *reptation time*, the time τ_d for disengagement from the tube, is proportional to $M^2/M^{-1} = M^3$. Hence, the longest relaxation time, $\tau_1 = \tau_d$, is predicted to be proportional to M^3 , not too different from the measured scaling law, $\tau_1 \sim M^{3.4 \pm 0.1}$.

The diameter, a , of the tube corresponds to the entanglement spacing, M_e . That is, a strand of polymer having molecular weight M_e spans a random walk end-to-end distance a (Fig. 3-24). Thus, $\langle R^2 \rangle_0 = a^2 M / M_e$, and

$$a^2 = \frac{4}{5} \frac{\rho N_A k_B T \langle R^2 \rangle_0}{M G_N^0}$$

The tube itself is a random walk, each step of which has length a . This random walk is called the "primitive path" of the chain. The contour length of the tube, or the primitive path, is therefore $L_t = aM/M_e$. For polymers of high molecular weight, the tube's contour length is much less than the contour length of the chain (see Fig. 3-24). Thus, the chain meanders about the primitive path. Some values for the tube diameter a for typical polymer melts are presented in Table 3-3.

3.7.2 Nonreptative Relaxation Mechanisms

The reptation theory has been controversial. In large part, this is because experimental data and computer simulations usually show some deviations from the behavior expected for pure

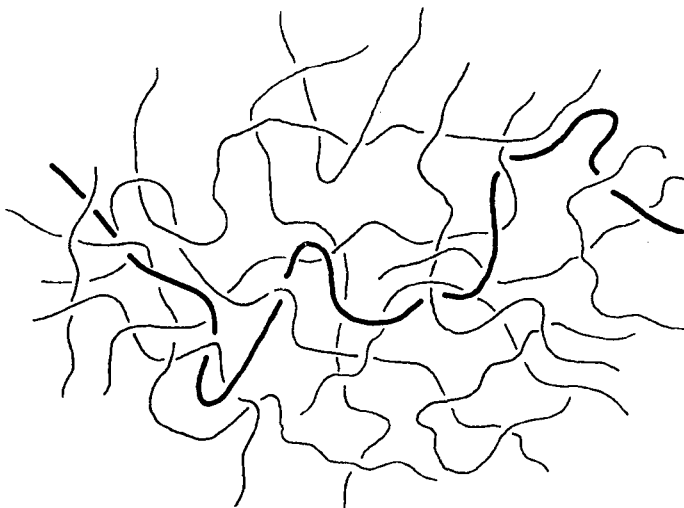


Figure 3.23 A polymer molecule entangled in a mesh of other polymer chains. (From Graessley 1982, reprinted with permission from Springer Verlag.)

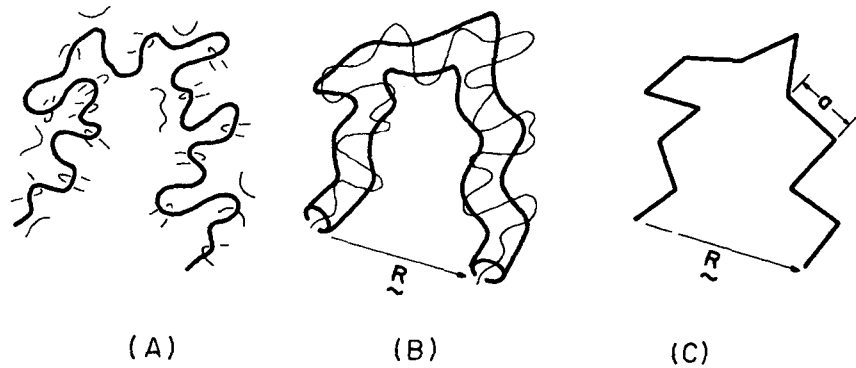


Figure 3.24 (A) A polymer molecule is entangled with neighboring molecules that (B) confine the given chain to a tube-like region. (C) The tube contour is roughly that of a random walk with step size equal to the tube diameter, a . This random walk is called the *primitive path*; its contour length is much less than the contour length of the chain itself. (From Graessley 1982, reprinted with permission from Springer Verlag.)

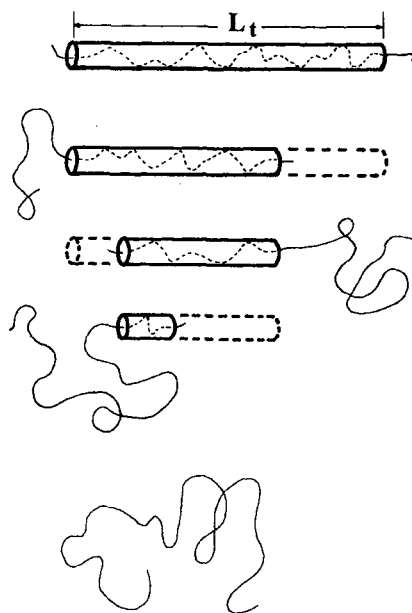


Figure 3.25 Reptation of a polymer molecule out of its tube, where, to aid visualization, the tube of Fig. 3-24 has been “straightened out.” (From Graessley 1982, reprinted with permission from Springer Verlag.)

reptation. A prime example is the observed 3.4 power law for the viscosity (Kröger 1995), which differs somewhat from the predicted 3.0 power law (Doi 1983). It has gradually been realized that these deviations are due to relaxation processes other than reptation that are important in all but the most extreme cases of high molecular weight, low polydispersity, and slow flow. Thus, a satisfactory theory for flow and relaxation of entangled polymers

needs to account for the nonreptative processes. The most important of these are *primitive-path fluctuations* and *constraint release*. In the highly nonlinear regime of strong flows, one must also account for *tube stretching*, discussed in Section 3.7.5.2.

3.7.2.1 Primitive-Path Fluctuations

This mechanism is most easily described for the case of an entangled polymer chain tethered at one end—for example, to a polymer branch point. In this situation, the entangled chain cannot slide back and forth as a whole, and hence it cannot reptate. de Gennes (1975) and Doi and Kuzuu (1980) proposed that the chain then relaxes by *primitive-path fluctuations*, sometimes called “breathing modes.” In this mechanism, fluctuations draw the end of the chain in from the end of the tube (see Fig. 3-26). When the molecule re-expands, the end portion of the tube is forgotten, and the stress associated with the chain ends is lost. For complete relaxation to occur by this mechanism, the free end of the chain must diffuse to the tether point, and from there re-extend into a new tube. This diffusion process is entropically unfavorable, since it involves configurations that are ever more improbable as the size of the fluctuation increases [see Fig. 3-26 (bottom)]. Hence, the time for this process increases *exponentially* with the distance along the tube that the diffusion must occur. Using scaling arguments, Doi and Kuzuu (1980) predicted that the relaxation time $\tau(x)$ for a chain segment a fractional distance x from the tether point to relax is

$$\tau(x) = \tau_0(x) \exp \left[\frac{3}{2} \frac{M}{M_e} (1-x)^2 \right] \quad (3-65)$$

where τ_0 is a time scale that is in principle dependent on x (Doi and Edwards 1986). This dependence is much weaker than that in the exponential; as a rough estimate, τ_0 is sometimes taken to be a constant, the Rouse relaxation time of the chain. A more accurate formula for $\tau_0(x)$ can be found in Milner and McLeish (1997). [Also, the factor of 3/2 in the exponential is changed to 15/8 if the entanglement spacing M_e is defined in Eq. (3-63) without the factor of 4/5.] According to Eq. (3-65), the segment of the chain at the tether point ($x = 0$) relaxes in a time longer than that of the free end ($x = 1$) by an exponential in the number of entanglements. Since the segments at intermediate positions

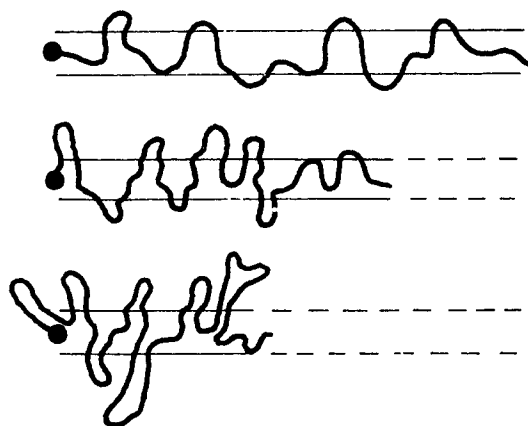


Figure 3.26 A fluctuation of the primitive-path length occurs when a chain randomly pulls its end away from the end of the tube. The probability of such a fluctuation decreases exponentially with the size of the fluctuation. (From Graessley 1982, reprinted with permission from Springer Verlag.)

have intermediate relaxation times, primitive-path fluctuations obviously create a very wide distribution of relaxation times. Also, since the zero-shear viscosity η_0 scales as the longest relaxation time, η_0 increases exponentially with the molecular weight, a prediction that has been confirmed experimentally in “star” branch polymers (Pearson and Helfand 1984).

If both ends of the molecule are free to move, and so the chain can reptate, segments in the interior of the chain will relax faster by reptation than by primitive-path fluctuations, and so reptation will control the longest relaxation time of the chain. However, because primitive-path fluctuations are so much faster for the chain ends than for the chain center, the chain ends will still relax by primitive-path fluctuations. Only for very high molecular weights ($M/M_e \gtrsim 100$) are the contributions of fluctuations confined to small enough portions of the chain ends that these effects can be neglected.

3.7.2.2 Constraint Release

Another important relaxation process in entangled melts is *constraint release*, depicted in Fig. 3-27. When an end of a surrounding chain moves past a “test” chain, an entanglement constraint restricting the motion of the test chain is released, and a portion of the latter is freed to reorient (Graessley 1982; Montfort et al. 1986; Pearson 1987; Viovy et al. 1991). Constraint release can only be completely neglected for the case of an isolated chain

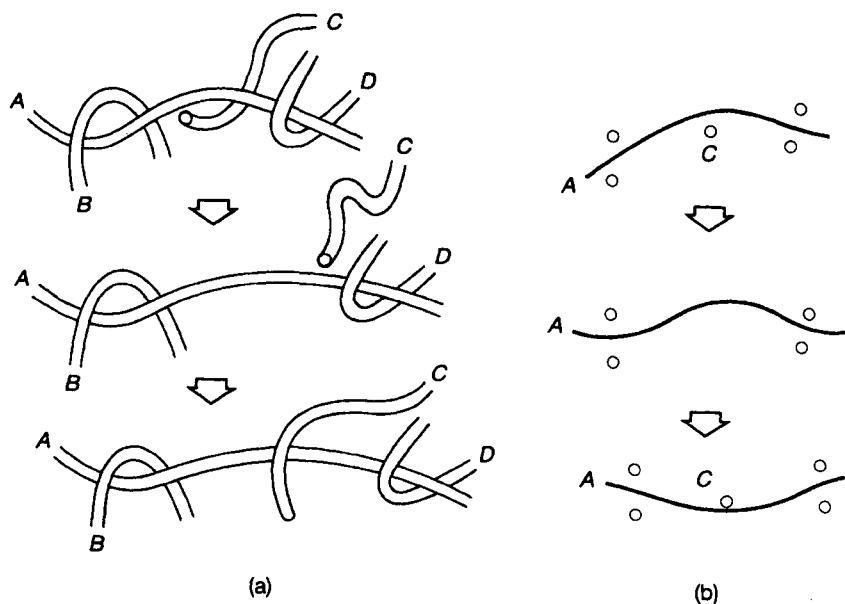


Figure 3.27 Depiction of the “constraint-release” mechanism of relaxation. In (a), the topological constraint imposed on chain A by chain C is released, as the end of chain C crosses under chain A. Even if C eventually re-entangles with A, chain A has been given a chance to change its orientation, as illustrated in the two-dimensional depiction in (b) (From Doi and Edwards, copyright © 1986 by Oxford University Press, Inc. Used by permission of Oxford University Press, Inc.)

entangled with a matrix that is cross-linked, or whose molecular weight is higher than that of the test chain. Neglect of constraint release is marginally valid for monodisperse chains undergoing slow flows, but is grossly inaccurate for long chains entangled with shorter chains, since the shorter chains can release constraints by diffusing faster than the long chain can reptate.

3.7.3 Evidence for Reptation

Despite these complications, there are now numerous evidences that the tube model is basically correct. The signatory mark that the chain is trapped in a “tube” is that the chain ends relax first, and the center of the chain remains unrelaxed until relaxation is almost over. Evidence that this occurs has been obtained in experiments with chains whose ends are labeled, either chemically or isotopically (Ylitalo et al. 1990; Russell et al. 1993). These studies show that the rate of relaxation of the chain ends is distinctively faster than the middle of the chain, in quantitative agreement with reptation theory. The special role of chain ends is also shown indirectly in studies of the relaxation of “star” polymers. Stars are polymers in which several branches radiate from a single branch point. The arms of the star cannot reptate because they are anchored at the branch point (de Gennes 1975). Relaxation must thus occur by the slower process of primitive-path fluctuations, which is found to slow down exponentially with increasing arm molecular weight, in agreement with predictions (Pearson and Helfand 1984).

Perhaps the most graphic evidence of the validity of reptation-related ideas is to be found in the experiments of Chu and coworkers (Perkins et al. 1994a). They observed directly through a microscope the relaxation processes of very long ($\sim 16\text{--}100\ \mu\text{m}$) fluorescently stained DNA molecules entangled in a sea of other, untagged—and therefore invisible—molecules (see Fig. 3-4). These experiments show convincing visual evidence that molecular motion is confined to a tube-like region. Molecular dynamics (MD) simulations also show chain motion that is highly anisotropic, suggesting that the diffusive motion of a long molecule is largely confined to a tube [see Fig. 3-28 (Kremer and Grest 1990)].

A variety of other experiments, measuring time-dependent pair correlation functions (Richter et al. 1992), diffusion coefficients (Tirrell 1984; Lodge et al. 1990), and viscoelastic relaxation phenomena, are more-or-less consistent with reptation theories. Complete quantitative agreement with simple reptation theories is rarely obtained, however, presumably because of additional mechanisms, such as “constraint release” and “primitive-path fluctuations,” that occur along with pure reptation. Lodge et al. (1990) have published a comprehensive status report on the extent to which reptation theory is in agreement with experimental data on viscosity, diffusion, stress relaxation, gel electrophoresis, and other measurements. Since the main focus of this book is the prediction of rheological properties, we shall in the remainder of the chapter describe the predictions of “tube” theories for rheological properties, starting with the Doi–Edwards constitutive equation.

3.7.4 The Doi–Edwards Constitutive Equation

Doi and Edwards (1978a, 1979, 1986) developed a constitutive equation for entangled polymeric fluids that combines the linear viscoelastic response predicted by de Gennes

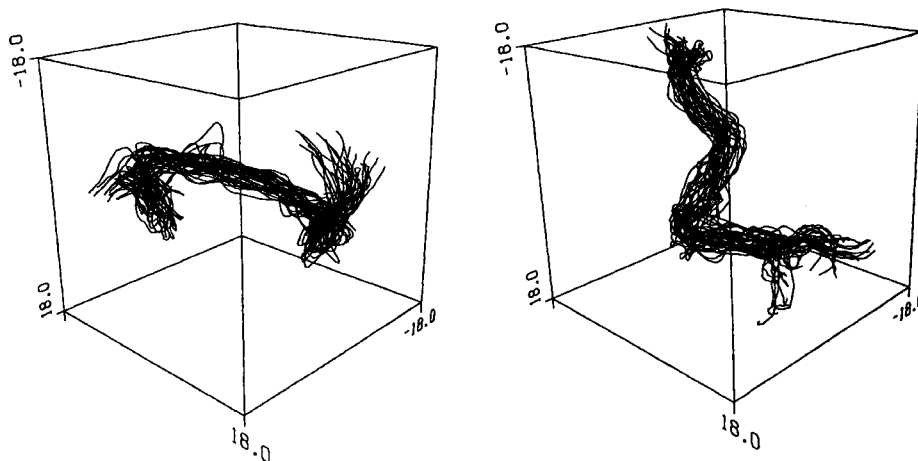


Figure 3.28 Each of the two images contains superimposed configurations of a chain at many different instants in time in a molecular-dynamics simulation of a melt of such chains in a box. Over the time scale simulated, each chain appears to be confined to a tube-like region of space, except at the chain ends. (From Kremer and Grest, reprinted with permission from *J. Chem. Phys.* 92:5057, Copyright 1990 American Institute of Physics.)

for a reptating chain with a nonlinear response to large deformations. Although the Doi-Edwards theory neglects primitive-path fluctuations and constraint release, and therefore is not quantitative, it is a good starting point for understanding the behavior of entangled melts and solutions.

3.7.4.1 Linear Relaxation Modulus

Consider a chain in a tube at time zero. Analysis of the reptation process (de Gennes 1971) shows that after a time t , only a fraction $P(t)$ of the original tube remains unvacated, namely

$$P(t) = \sum_{i \text{ odd}} \frac{8}{\pi^2 i^2} \exp\left[-\frac{i^2 t}{\tau_d}\right] \quad (3-66)$$

The linear relaxation modulus is $P(t)$ times G_N^0 :

$$G(t) = \sum_{i \text{ odd}} G_i \exp[-t/\tau_i], \quad G_i = 8G_N^0/\pi^2 i^2, \quad \tau_i = \tau_d/i^2 \quad (3-67)$$

The storage and loss moduli, G' and G'' , are obtained from the relaxation spectrum in the usual way—that is, using $G' = \sum G_i [\omega^2 \tau_i^2 / (1 + \omega^2 \tau_i^2)]$; $G'' = \sum G_i [\omega \tau_i / (1 + \omega^2 \tau_i^2)]$. The longest relaxation mode of the relaxation modulus in Eq. (3-67) is the dominant one; it accounts for 96% of the zero-shear viscosity. Thus, the reptation model predicts that for a nearly monodisperse melt, the relaxation spectrum is dominated by a single relaxation time, $\tau_1 = \tau_d$. This is in reasonable accord with experimental data at low and moderate frequencies (see the dashed line in Fig. 3-29). As the frequency increases, however, there

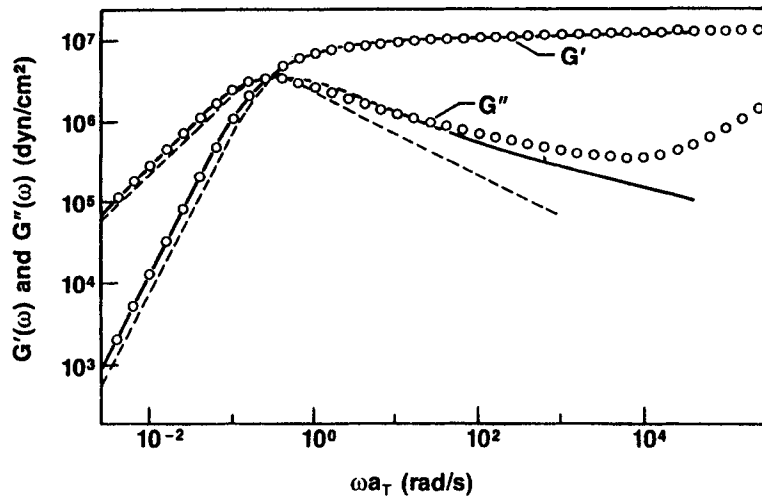


Figure 3.29 Linear moduli G' and G'' versus frequency shifted via time-temperature superposition to 27°C for a polybutadiene melt of molecular weight 360,000 and of low polydispersity. The dashed line is the prediction of reptation theory given by Eq. (3-67); the solid line includes effects of fluctuations in the length of the primitive path. (From Pearson 1987.)

is more deviation from the Doi-Edwards model, apparently because reptation is the only relaxation process considered. Any additional relaxation processes that might be present will tend to broaden the spectrum, thereby bringing $G'(\omega)$ and $G''(\omega)$ closer to the experimental curves. Inclusion of the process of tube fluctuation, for example, removes most of the discrepancy between experiment and theory (Pearson 1987; Milner and McLeish 1998) but does not account for the upturn in G'' at high ω (see the solid line in Fig. 3-29). This upturn is apparently caused by Rouse-like motions of parts of the molecule that lie within a primitive-path step (Milner and McLeish 1998). Even small levels of polydispersity broadens the relaxation spectrum (Lin 1984), and so does constraint release.

3.7.4.2 Nonlinear Modulus and Damping Function

Figure 3-30a shows the *nonlinear* modulus, $G(t, \gamma)$ after a series of “step” strains, γ , suddenly imposed on a concentrated polystyrene solution (Einaga et al. 1971). The nonlinear modulus is just the stress divided by the strain. Figure 3-30b shows that vertical shifting brings the relaxation moduli for various γ into coincidence at times greater than $\tau_r \sim 20$ sec. Thus, at times longer than τ_r , $G(t, \gamma)$ is factorable into time- and strain-dependent functions: $G(t, \gamma) = G(t)h(\gamma)$, where $G(t)$ is the linear modulus and $h(\gamma)$ is a strain-dependent *damping function*. The damping function, $h(\gamma)$, plotted in Fig. 3-31, shows considerable *strain softening*; that is, h decreases with increasing γ . The temporary network model of Green and Tobolsky (Section 3.4.4), on the other hand, has no strain softening since it predicts that $h(\gamma) = 1$ for all γ .

Doi and Edwards (1978a, 1979) explained this strain softening using an extension of the tube model of de Gennes. Suppose that the melt is subjected to a step strain and

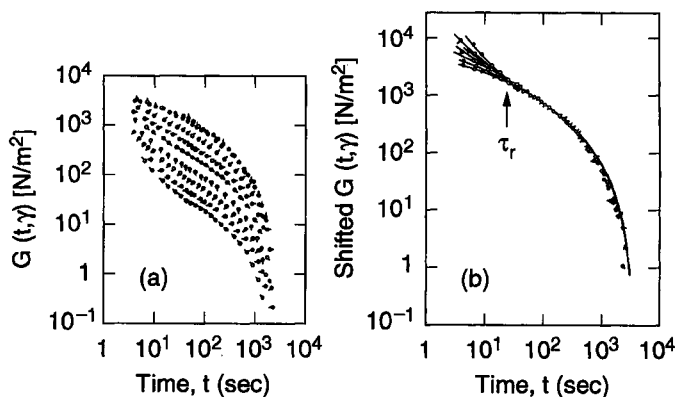


Figure 3.30 (a) The nonlinear shear relaxation modulus $G(t, \gamma)/\gamma$ as a function of time for various strain amplitudes for a 20% concentrated solution of polystyrene of molecular weight 1.8×10^6 in chlorinated diphenyl. Each curve corresponds to a different strain, ranging from 0.41 to 25.4, with the lower curves corresponding to the higher strains. (b) The curves are superimposed at times longer than $\tau_r = 20$ sec via vertical shifting by an amount $h(\gamma)$ plotted in Fig. 3-31. (From Einaga et al. 1971, with permission from the Society of Polymer Science, Japan.)

that the tube and the chain it contains are stretched affinely. Although the tube prevents lateral motion of the molecule, it does not stop the molecule from *retracting* along the tube contour. Since retraction does not violate the tube constraints, it occurs quickly compared to reptation. Specifically, retraction occurs in a time roughly equal to the Rouse time τ_r for the whole chain, which is smaller than τ_d by the ratio $\tau_r/\tau_d = (N_e/3N)$, where N/N_e is the number of entanglements per chain (Doi and Edwards 1986). (An even faster time scale than τ_r is the time for relaxation of the portion of a chain within a tube segment; this happens by Rouse-like processes in an *equilibration time* $\tau_e = a^4 \zeta_0 / k_B T b^2$). The retraction of the chain brings the contour length of its primitive path back to its equilibrium value aM/M_e . The nonfactorable relaxation seen in Fig. 3-30 at times shorter than τ_r is presumed to be caused by incomplete retraction. At times longer than τ_r , retraction is complete; the remaining stress must relax by reptation, which occurs on a longer time scale. The strain softening in $h(\gamma)$ is therefore attributed to the retraction process.

Retraction moves a strand from one part of the tube to another; hence the strand's orientation is determined not by the orientation of the part of the tube it originally occupied, but by the orientation of the part of the tube into which it moves. To simplify the problem, however, Doi and Edwards invoked the *independent alignment approximation*, which assumes that after retraction each *strand is oriented independently of the others*, and the change in orientation produced by retraction is neglected.

Since the retraction process keeps the overall primitive path length constant, if one invokes the independent alignment approximation, each step in the primitive path returns to the same length, a , after retraction. The net effect of the deformation, therefore, is to *orient strands without stretching them*. Since rigid rods also respond to a deformation by rotating without stretching, the Doi-Edwards constitutive equation for melts is similar to that for the elastic stress for rigid-rod molecules [see Section 6.3.2.1 and Doi and Edwards (1978b)].

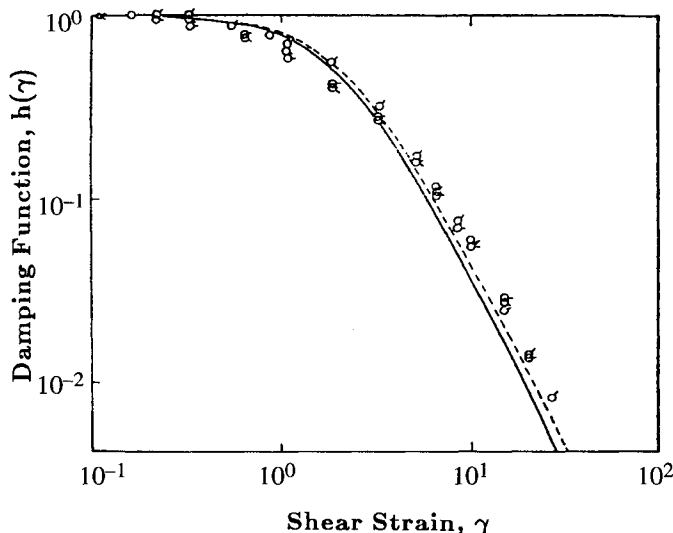


Figure 3.31 Damping function $h(\gamma)$ obtained by vertically shifting the time-dependent nonlinear moduli in Fig. 3-30a into superposition at long times. The data are from Fukuda et al. (1975). The solid and dashed lines are the prediction of the Doi–Edwards model, respectively, with and without the independent alignment approximation. (From Doi and Edwards 1978a, reproduced by permission of The Royal Society of Chemistry.)

3.7.4.3 Stress Tensor After a Step Strain

In the original Doi–Edwards model, retraction is assumed to occur infinitely fast. The stress tensor is then given by the “elastic,” or Brownian, stress for rigid rods [see Eq. (6-36)]:

$$\boldsymbol{\sigma} = 3\nu k_B T \langle \mathbf{u}\mathbf{u} \rangle = 3\nu k_B T a^{-2} \langle \mathbf{R}\mathbf{R} \rangle \quad (3-68)$$

where \mathbf{u} is the unit vector parallel to the end-to-end vector of a strand (or a step of the primitive path), a is the length of a step of the primitive path, and the brackets “ $\langle \rangle$ ” denote an average over all strands. This expression for $\boldsymbol{\sigma}$ satisfies the stress-optic law.

Although the expression for the stress tensor in the Doi–Edwards model is the same as that of the temporary network model, except for the coefficient $3\nu k_B T a^{-2}$ [see Eq. (3-13)], the nonlinear response of a polymer strand to a step strain is different. In the temporary network model, $\mathbf{R} = \mathbf{R}' \cdot \mathbf{E}$, where \mathbf{R} and \mathbf{R}' are the strand’s end-to-end vectors before and after the deformation, and \mathbf{E} is the *inverse deformation gradient* tensor, defined in Eq. (1-12). In the Doi–Edwards theory, on the other hand, $\mathbf{R} = \mathbf{R}' \cdot \mathbf{E} / |\mathbf{u}' \cdot \mathbf{E}|$; thus, the strand’s length $|\mathbf{R}| = |\mathbf{R}'|$ remains constant because of retraction. Hence, in the Doi–Edwards theory, after a step strain and after retraction, but before reptation occurs, the stress is given by

$$\boldsymbol{\sigma} = 3\nu k_B T \langle \mathbf{u}\mathbf{u} \rangle = 3\nu k_B T \left\langle \frac{\mathbf{u}' \cdot \mathbf{E} \mathbf{u}' \cdot \mathbf{E}}{|\mathbf{u}' \cdot \mathbf{E}|^2} \right\rangle_0 = \frac{3}{5} \nu k_B T \mathbf{Q} \quad (3-69)$$

where “ $\langle \cdot \rangle_0$ ” averages over an isotropic distribution of the unit vector \mathbf{u}' so that $\psi_0(\mathbf{u}') = 1/4\pi$; thus

$$\langle \cdot \rangle_0 = \int \frac{d^2\mathbf{u}}{4\pi} = \int_0^\pi \int_0^{2\pi} \cdot d\phi \sin\theta d\theta$$

where $\mathbf{u}' = (\sin\theta \cos\phi, \sin\theta \sin\phi, \cos\theta)$. In Eq. (3-69), \mathbf{Q} is defined as

$$\mathbf{Q} \equiv 5 \left\langle \frac{\mathbf{u}' \cdot \mathbf{E} \mathbf{u}' \cdot \mathbf{E}}{|\mathbf{u}' \cdot \mathbf{E}|^2} \right\rangle_0 \quad (3-70)$$

The factor of 5 is introduced into the definition of \mathbf{Q} so that \mathbf{Q} equals the linear viscoelastic strain, $\boldsymbol{\gamma}$, when the strain is small. $G_N^0 = 3/5\nu k_B T$ is then the plateau modulus. When the independent alignment approximation is dropped, this is corrected to $G_N^0 = 4/5\nu k_B T$.

In a step shear, Q_{12} , the shearing component of \mathbf{Q} (where “1” is the flow direction and “2” is the gradient direction), can be expressed as $\gamma h(\gamma)$, where $h(\gamma)$ is the “damping function” defined earlier. Figure 3-31 shows that the predicted damping function agrees well with the experimental damping function for monodisperse polystyrene solutions. Figure 3-31 also shows that the damping function in a step shear is not much affected by the “independent alignment approximation.” For other deformation histories, such as a “double-step” strain, however, larger errors are introduced by the independent alignment approximation (Doi and Edwards 1986). Damping functions can also be defined for other single-step-strain deformations, such as step biaxial extension and step uniaxial extension; for these, experimental data for nearly monodisperse melts are also in reasonably good agreement with the predictions of the Doi–Edwards theory (Urakawa et al. 1995).

3.7.4.4 Constitutive Equation

The stress that remains a time t after a step strain is the product of the stress immediately after the step, given by Eq. (3-69), multiplied by the fraction of tube length $P(t)$ vacated because of reptation, given by Eq. (3-66). If the strain is imposed gradually, so that reptation occurs during deformation, the stress is given by a *history integral*, analogous to the Lodge equation, (3-24). This history integral is the *Doi–Edwards constitutive equation*,

$$\boldsymbol{\sigma} = \int_{-\infty}^t m(t-t') \mathbf{Q}(t', t) dt' \quad (3-71)$$

where the memory function $m(t-t')$ is given by

$$m(t-t') \equiv \frac{d}{dt'} G(t-t')$$

and $G(t-t')$ and $\mathbf{Q}(t', t)$ are given by Eqs. (3-67) and (3-70), respectively.

Equation (3-71) can be expressed in the form

$$\boldsymbol{\sigma} = \int_{-\infty}^t m(t-t') [\phi_1(I_1, I_2) \mathbf{B}(t', t) + \phi_2(I_1, I_2) \mathbf{C}(t', t)] dt' \quad (3-72)$$

where \mathbf{C} is the *Cauchy tensor*, which is the inverse of the Finger tensor, $\mathbf{C} \equiv \mathbf{B}^{-1}$; I_1 is the trace of the Finger tensor \mathbf{B} , and I_2 is the trace of its inverse \mathbf{C} . For the special case of a

separable K-BKZ equation (Kaye 1962; Bernstein et al. 1963), the functions ϕ_1 and ϕ_2 are related to a strain energy function, $U(I_1, I_2)$, by

$$\phi_1 \equiv 2 \frac{\partial U}{\partial I_1}, \quad \phi_2 \equiv -2 \frac{\partial U}{\partial I_2}$$

See Tanner (1985) or Larson (1988) for more details about the K-BKZ category of constitutive equations.

The Doi-Edwards equation is a special case of a separable K-BKZ equation, for which Currie (1980) found an accurate analytic approximation, namely

$$U(I_1, I_2) \approx \frac{5}{2} \ln \left(\frac{J-1}{7} \right) \quad (3-73)$$

with

$$J \equiv I_1 + 2(I_2 + 13/4)^{1/2} \quad (3-74)$$

From this potential function, one obtains

$$\mathbf{Q} \approx \left(\frac{5}{J-1} \right) \mathbf{B} - \left(\frac{5}{(J-1)(I_2 + 13/4)^{1/2}} \right) \mathbf{C} \quad (3-75)$$

A simpler and cruder approximation is (Larson 1984a)

$$U \sim 5/2 \ln(1 + 1/5(I_1 - 3)) \quad (3-76a)$$

which gives

$$\mathbf{Q} = \left(\frac{1}{1 + 1/5(I_1 - 3)} \right) \mathbf{B} \quad (3-76b)$$

This latter approximation shows that the strain dependence of the Doi-Edwards equation is “softer” than that of the temporary network model roughly by the factor $1 + (I_1 - 3)/5$.

There is also a differential approximation to the Doi-Edwards equation (Marrucci 1984; Larson 1984b):

$$\overset{\nabla}{\boldsymbol{\sigma}} + \frac{2}{3G} \mathbf{D} : \boldsymbol{\sigma} \boldsymbol{\sigma} + \frac{1}{\tau} (\boldsymbol{\sigma} - G\boldsymbol{\delta}) = \mathbf{0} \quad (3-77)$$

Equation (3-77) differs from the upper-convected Maxwell equation, Eq. (3-32), in that it includes the term $(2/3G)\mathbf{D} : \boldsymbol{\sigma} \boldsymbol{\sigma}$, which imparts strain softening and shear thinning to the behavior of the model.

3.7.5 Predictions of Reptation Theories

3.7.5.1 Steady-State Shear and Extension

The uniaxial extensional viscosity $\bar{\eta}(\dot{\epsilon})$ and the viscometric functions $\eta(\dot{\gamma})$ and $\Psi_1(\dot{\gamma})$, predicted by the Doi-Edwards model for monodisperse melts, are shown in Fig. 3-32. The Doi-Edwards model predicts extreme thinning in these functions; the high-shear-rate asymptotes scale as $\bar{\eta} \propto \dot{\epsilon}^{-1}$, $\eta \propto \dot{\gamma}^{-1.5}$, and $\Psi_1 \propto \dot{\gamma}^{-2}$. The second normal

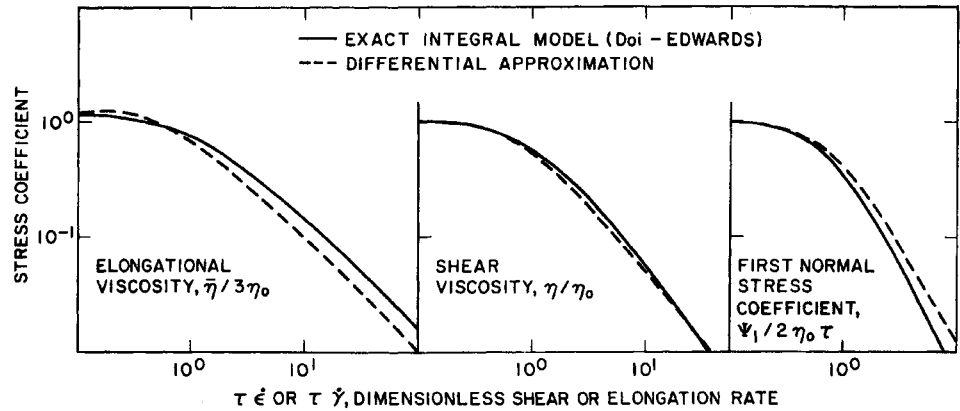


Figure 3.32 The predictions of the Doi–Edwards integral model for the normalized uniaxial extensional (or elongational) viscosity $\bar{\eta}$ and for the viscometric shear coefficients $\eta(\dot{\gamma})$ and $\Psi_1(\dot{\gamma})$. Also shown are the predictions of the differential model, Eq. (3-77). (From Larson, 1984b, with permission from the Journal of Rheology.)

stress coefficient, not shown in Fig. 3-32, scales as $\Psi_2 \propto -\dot{\gamma}^{-2.5}$ at high shear rates (Doi and Edwards 1979). The predicted shear thinning is so severe that as the shear rate increases, the shear stress $\eta\dot{\gamma}$ is predicted to pass through a maximum and then *decrease* with further increases in $\dot{\gamma}$ (see Fig. 3-33). Hence, at each shear stress there are at least *two* values of the shear rate. This, it is predicted, should lead to *material instabilities*—that is, apparent slip phenomena, such as “spurt,” sometimes observed in flow through capillaries (see Section 3.7.5.3).

Experimentally, melts of low polydispersity that do not overtly “spurt,” “slip,” or succumb to other material instabilities will typically show steeply decreasing values of the viscosity and first normal stress coefficient in the shear-thinning region. Menezes and Graessley (1980) reported that $\eta \propto \dot{\gamma}^{-0.82}$ and $\Psi_1 \propto \dot{\gamma}^{-1.5}$ at large $\dot{\gamma}$. These dependencies become steeper as the polymer becomes more entangled, so that the power-law exponent for η approaches -1 , implying that the shear stress is almost constant at high shear rate, as shown by the open triangles in Fig. 3-34. However, there is no direct evidence that η and Ψ_1 ever fall as steeply with shear rate as predicted by the Doi–Edwards theory. This is most likely

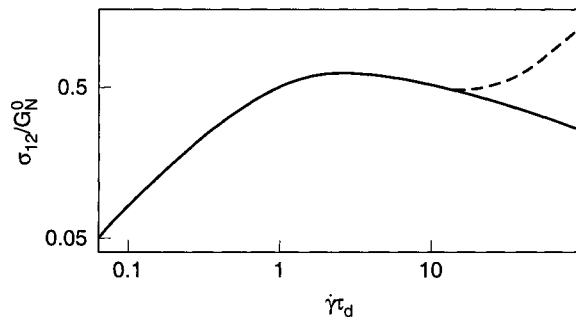


Figure 3.33 The solid curve is the dimensionless shear stress σ_{12}/G_N^0 versus dimensionless shear rate $\dot{\gamma}\tau_d$ predicted by the Doi–Edwards constitutive equation, Eq. (3-71). The dashed curve adds a speculated contribution to the stress from Rouse modes. (From Doi and Edwards 1979, reproduced by permission of The Royal Society of Chemistry.)

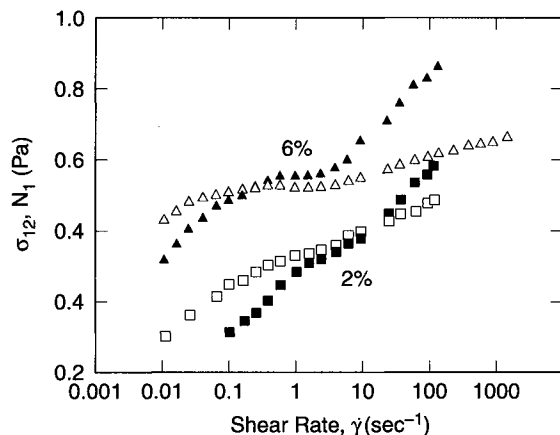


Figure 3.34 Shear stress (open symbols) and first normal stress difference (closed symbols) as functions of shear rate for two solutions of very-high-molecular-weight polymethylmethacrylate ($M = 23.8 \times 10^6$) in toluene at a concentration of 2 g/dL (squares) and 6 gm/dL (triangles). (From Bercea et al. 1993, with permission.)

because processes of relaxation other than reptation occur. In particular, Marrucci (1996) and Marrucci and Ianniruberto (1997) have pointed out that fast flows ($De \gg 1$) convect away the polymer molecules constraining a given chain, and therefore destroy the tube surrounding that chain, faster than the chain itself can reptate out of the tube. Under these conditions, “convective constraint release,” not reptation, is probably the dominant mechanism of relaxation. A new theory incorporating “convective constraint release” and “tube stretching” into the Doi–Edwards model predicts a nearly constant shear stress as a function of shear rate in the high shear rate regime [see Fig. 3-35 (Marrucci and Ianniruberto 1997; Larson et al. 1998)]. The predictions of this theory agree with many rheological measurements in both steady-state and transient shear flows (compare, for example, Fig. 3-35 with Fig. 3-34). The equations for this new theory are given and discussed in Problem 3.10.

The Doi–Edwards equation predicts that the ratio Ψ_2/Ψ_1 is $-2/7 = -0.29$ at low shear rates. This changes to $\Psi_2/\Psi_1 = -1/7 = -0.14$ when the “independent alignment approximation” is dropped (Osaki et al. 1981). With or without the independent alignment approximation, the ratio $-\Psi_2/\Psi_1$ is predicted to decrease towards zero as the shear rate increases. The prediction of Ψ_2/Ψ_1 for entangled solutions contrasts with that predicted for dilute solutions, for which Ψ_2/Ψ_1 is close to zero over the whole range of shear rates (see Fig. 3-36). These predictions for dilute and entangled solutions have been confirmed qualitatively in experiments of Magda et al. (1993) and Brown et al. (1995). Figure 3-37 shows Ψ_2/Ψ_1 versus an approximate Weissenberg number N_1/σ_{12} for a series of polystyrene solutions of high molecular weight, at concentrations ranging from dilute to concentrated. The data fall into two distinct groups, depending on the concentration: For the dilute solutions, $-\Psi_2/\Psi_1 \approx 0$, as predicted, while for the entangled solutions, $-\Psi_2/\Psi_1 \approx 0.2$ at low shear rates, decreasing toward zero as the shear rate increases. The measured ratios of $-\Psi_2/\Psi_1$ are in qualitative agreement with the predicted ones (compare Fig. 3-36 with Fig. 3-37). In concentrated solutions or melts of molecular weight low enough that the molecules are *unentangled*, one might expect the prediction of the Rouse theory to apply, namely $\Psi_2/\Psi_1 = 0$ for all shear rates. However, both experiments (Magda et al. 1993) and molecular dynamics simulations (Berker et al. 1992; Kröger et al. 1993) for unentangled solutions and melts give surprisingly high values of $-\Psi_{2,0}/\Psi_{1,0}$, around 0.15–0.45 or so, at low shear rates.

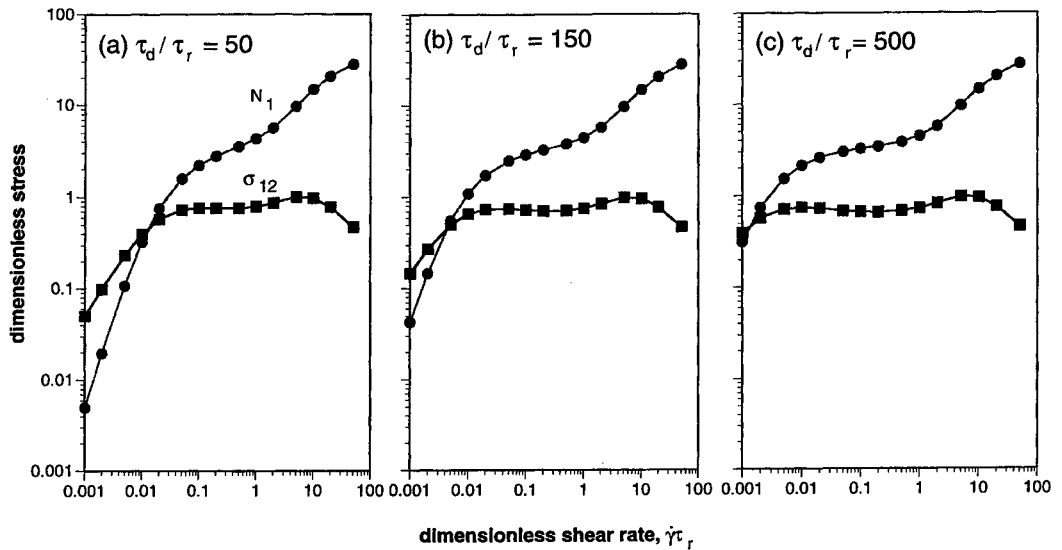


Figure 3.35 Steady-state values of the reduced shear stress σ_{12}/G_N^0 and first normal stress difference N_1/G_N^0 as functions of dimensionless shear rate $\dot{\gamma}\tau_r$ predicted by the equations of a constraint-release reptation theory (see Problem 3.10) for $\tau_d/\tau_r =$ (a) 50, (b) 150, and (c) 500, where τ_d is the reptation time and τ_r is the Rouse retraction time. See also Marrucci and Ianniruberto (1997). (From Larson et al. 1998, with permission.)

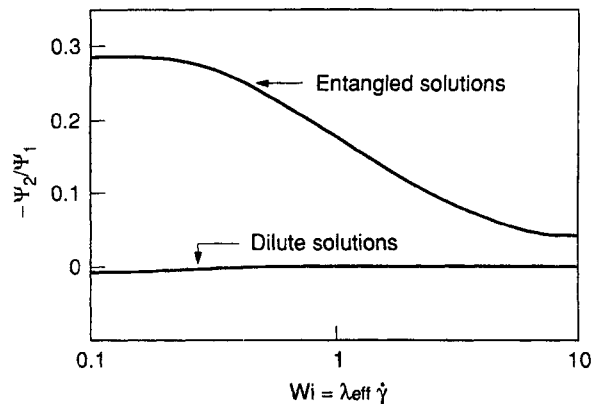


Figure 3.36 Negative ratio of the second to the first normal stress coefficients versus Weissenberg number predicted for entangled polymers by the Doi–Edwards theory, and for dilute solutions by the bead-spring theory with conformation-dependent hydrodynamic interaction. Here $\tau_{\text{eff}} \equiv \Psi_{1,0}/2\eta_{p,0}$. (Reprinted with permission from Magda et al., *Macromolecules* 26:1696. Copyright 1993, American Chemical Society.)

3.7.5.2 Stress Overshoots

The Doi–Edwards equation predicts an overshoot in shear stress as a function of time after inception of steady shearing, but no overshoot in the first normal stress difference (Doi and Edwards 1978a). Typical overshoots in these quantities for a polydisperse melt are shown in Fig. 1-10. For monodisperse melts, the Doi–Edwards model predicts that the shear-stress maximum should occur at a shear strain $\dot{\gamma}t = \gamma_p$, of about 2, roughly independently of

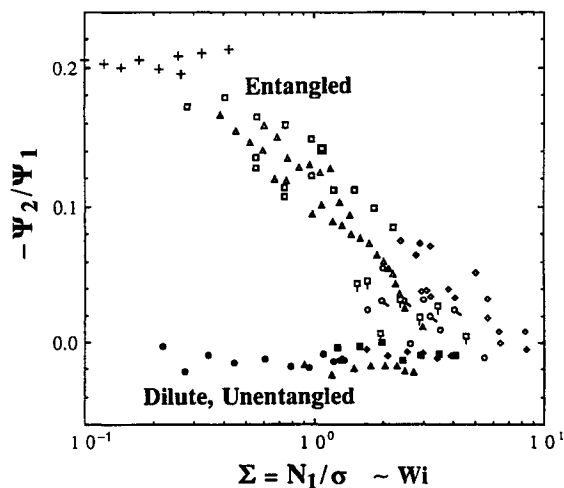


Figure 3.37 Negative ratio of the second to the first normal stress coefficients versus stress ratio N_1/σ for various dilute solutions (concentration ≤ 0.6 wt%; closed symbols) and entangled solutions (concentration ≥ 1 wt%; open symbols). (Reprinted with permission from Magda et al., *Macromolecules* 26:1696. Copyright 1993, American Chemical Society.)

the shear rate. For low strain rates, the experimental maximum is indeed at $\gamma_p \sim 2$; but for high strain rates it shifts to higher strains (Menezes and Graessley 1982). In addition, experiments show an overshoot in the first normal stress difference, which is *not* predicted by the Doi–Edwards equation; it occurs at a strain of about 5 at low shear rate. It has been observed that the strains at which these two overshoots occur increase with increasing shear rate when the shear rate exceeds the reciprocal of the *retraction time* τ_r (Menezes and Graessley 1982).

This behavior can be predicted if the Doi–Edwards theory is extended to allow for *tube stretching* (or incomplete retraction) (Marrucci and Grizzuti 1988; Pearson et al. 1991; Mead and Leal 1995; Larson et al. 1998). When shearing starts with $\dot{\gamma}\tau_r \gtrsim 1$, the polymer strands are stretched for a brief period, and the shear stress rises to a maximum. As the strands become highly oriented, their projected length in the direction of the shear gradient decreases, and the velocity difference between one end of the strand and the other begins to decrease. As a result, the shearing flow “loses its grip” on the molecules, and they are able to retract within their tubes. The first normal stress difference therefore overshoots and decreases towards its steady-state value. Equations that describe this tube-stretching process were presented in Pearson et al. (1991), and they are incorporated into the equations in Problem 3.10. They predict the shifting of the shear and normal stress maxima with shear rate.

3.7.5.3 Anomalous Rheology

As already noted, the measured nonlinear shear relaxation modulus, for linear molecules with little polydispersity, is in excellent agreement with the Doi–Edwards model at long times. However, for melts or concentrated solutions of very high molecular weight (e.g., $\phi M > 10^6$ for polystyrene, where ϕ is the polymer volume fraction), the measured damping function, $h(\gamma)$, is drastically lower than the Doi–Edwards prediction (Einaga et al. 1971; Vrentas and Graessley 1982; Larson et al. 1988; Morrison and Larson 1992). This anomalous

result seems surprising at first, since one expects that the Doi–Edwards theory should be most accurate for polymers having the highest entanglement density and, hence, the highest molecular weight. However, it has recently been shown that by using small particle probes within the fluid, the anomalous modulus is a consequence of *slippage* of the polymeric material either at, or within a few microns of, the solid surfaces between which the fluid is sheared (Archer et al. 1995). This behavior is not necessarily inconsistent with the Doi–Edwards theory. The Doi–Edwards theory predicts that at a fixed time after a step strain the shear stress has a maximum at a strain $\gamma_p \approx 2$, because of the extreme strain softening of the nonlinear modulus. From principles of mechanical stability, the shear stress maximum is expected to lead to *strain localization*, which is a kind of material instability. It occurs because the material can reduce its stress level by spontaneously increasing the strain in some regions of the sample and decreasing it in others (Marrucci and Grizzuti 1983; Kolkka et al. 1991). In this way, the strain in each region of the sample evolves toward a value that is either far above γ_p or far below it, and all regions of the sample develop a low stress level. If the highly strained regions are at the rheometer walls, apparent slip will be the result. Such “slip” can only occur in samples whose molecular weight is high enough that the retraction time is much shorter than the reptation time, $\tau_r \ll \tau_d$, so that a stress–strain curve with a stress maximum adequately describes the material’s rheology curve over a period of time long enough for strain localization to develop. Hence, anomalous “slip” produced by strain localization is expected (and observed) to be especially prominent for solutions and melts of high molecular weight (Marrucci and Grizzuti 1983).

A related phenomenon is predicted to occur in steady shearing flows (Doi and Edwards 1979). For such flows, the shear stress is predicted to exhibit a maximum as a function of shear rate (see Fig. 3-33). Thus, for each shear stress, there are two or more possible steady values of the shear rate; and a material instability, similar to slip, is again expected. Cates et al. (1993) have predicted that as a result of the material instability in a cone-and-plate or other simple shearing geometry, there should be a range of imposed shear rates over which the flow field becomes *stratified*; and two layers form, one with a high shear rate (on the dashed curve in Fig. 3-33) and the other with a low shear rate, but both having the same shear stress. As the imposed velocity V of the moving plate is increased, the shear rate in each of the two zones remains constant, but the thickness of the high-shear-rate layer increases at the expense of the low-shear-rate layer, so that the *average* shear rate is V/h , where h is the gap between the plates. Recent rheological data on very high molecular-weight ($M = 23.6 \times 10^6$) poly(methylmethacrylate) solutions (Bercea et al. 1993) are consistent with the theory of Cates et al., but direct confirmation of the two-layer flow has not yet been achieved in entangled polymer melts and solutions. Two-layer flow has been directly observed in flow of entangled “worm-like” micelles (Decruppe et al. 1995) (see Section 12.3.4.4). However, these solutions are complicated by the possibility that the two layers are induced by a flow-induced shift in the concentration at which a nematic phase appears.

It has also been suggested that a material instability, leading to stratified flow, is responsible for the so-called “spurt” phenomenon in which polymer melt flowing through a capillary suddenly increases its velocity by orders of magnitude when the pressure gradient crosses a critical threshold (McLeish and Ball 1986; McLeish 1987). However, theories for two-layer flows have generally ignored the role of “convective constraint release,” which probably has a large effect on these phenomena.

A somewhat different, though related, mechanism of slip in polymers of high molecular weight has been postulated by Brochard and de Gennes (1992). In their picture, polymer chains adsorbed to the rheometer surfaces become highly stretched and then disentangle from chains in the bulk, leading to a disentangled layer near the surfaces which has a very low viscosity compared to the bulk. Large shear gradients accumulate in this low-viscosity zone, leading to apparent slip. In the Brochard–de Gennes theory, the density of chains absorbed to the surface controls the critical stress level at which the apparent slip velocity becomes very large. Evidence supporting the Brochard–de Gennes picture has recently been put forth by Leger and coworkers (Migler et al. 1993), who used (a) glass surfaces treated to reduce chain adsorption and (b) an optical bleaching and evanescent-wave interference technique to measure slip within $0.1 \mu\text{m}$ of the glass surfaces.

Theories for “material instabilities” or “slip” in highly entangled melts and solutions are still under active development.

- Problems 3.7 through 3.11 test your ability to work with reptation ideas and the Doi–Edwards equation.

3.7.6 Effects of Polydispersity and Branching

3.7.6.1 Polydisperse Melts

Most polymeric fluids that are of commercial importance are highly polydisperse (values of M_w/M_n of 2 or more); and some, such as low-density polyethylene, have long-chain branching. It is important for many applications that these effects be accounted for in the constitutive equation. Using *constraint-release* ideas, reasonably accurate predictions have been made of the linear modulus of linear *bidispersed* melts—that is, mixtures of two chemically identical polymers having distinctly different molecular weights (Rubinstein et al. 1987). Constraint release is important in such bidispersed melts, because the relaxation of a long chain is accelerated by release of the entanglements it has with the shorter, faster-relaxing chains around it.

For continuous, rather than bidispersed, distributions of molecular weight, systematic accounting of reptation and constraint-release processes for all different chain lengths in the mixture becomes an impractically complex problem. A much simpler way to account not only for bidisperse molecular weight distributions, but also for continuous ones, has been proposed, using a semiempirical scheme called “double reptation” (Tsenoglou 1987; des Cloizeaux 1988; Tuminello 1986). The double-reptation scheme allows accurate prediction of G' and G'' from a specified molecular weight distribution (Wasserman and Graessley 1992). The “double-reptation” formula for the relaxation modulus $G_{\text{blend}}(t)$ of a blend containing a continuous weight distribution $W(M)$ of components is

$$\left(\frac{G_{\text{blend}}(t)}{G_N^0} \right)^{1/2} = \int_{M_e}^{\infty} W(M) F^{1/2}(M, t) dM \quad (3-78)$$

where $F(M, t)$ is the relaxation function $G(t)/G_N^0$ of a monodisperse melt of molecular weight M , and G_N^0 is the plateau modulus. Thus, if $G(t)/G_N^0$ is measured (or predicted) for monodisperse components, $G_{\text{blend}}(t)$ can be predicted using Eq. (3-78). The double-reptation scheme can also be applied in reverse to infer a molecular weight distribution from measurements of the linear modulus (Mead 1994). Since the rheology of a melt is often easier to measure than its molecular weight distribution, this method of estimating molecular weight distributions from rheological data is a very useful tool.

The intuitive idea behind double reptation is that an entanglement between two chains is released if the ends of either of the two chains reptates past the entanglement point. When this idea is applied to a monodisperse polymer, the relaxation function $F(t)$ within double reptation is proportional to the *square* of $P(t)$ given by Eq. (3-66). While this postulate is inconsistent with the theory of reptation as proposed by de Gennes, the idea can be thought of as a simple way of combining ordinary reptation with constraint release, and thus it has a reasonable physical motivation (Milner 1996; Mead 1996). Empirically, squaring the function $P(t)$ enriches the relaxation-time spectrum with extra time constants, and it leads to better agreement with experimental G' and G'' curves at frequencies above the terminal region, even for monodisperse melts.

3.7.6.2 Star Molecules

Ideas based on the tube model can predict the rheological properties of entangled melts of polymer molecules with a branched architecture. The simplest branched structure is the “star” polymer. As mentioned above, entangled star polymers cannot relax by reptation, since one end of each arm is anchored to a cross-link point. The arm therefore relaxes by primitive-path fluctuations (see Section 3.7.2.1). Now the tube constraining a test molecule is defined by its entanglements with surrounding molecules. But these surrounding molecules are themselves relaxing by primitive-path fluctuations. Since the branch tips of the surrounding molecules relax quickly, the constraints they impose on the test chain also disappear rather quickly. As a result, many of the constraints confining the portion of the test chain near the branch point will have been released by the time that portion of the test chain is ready to relax by primitive-path fluctuations, and thus the tube confining the portion of the test chain near the branch point will be *widened* by the time the chain in it relaxes (Ball and McLeish 1989; McLeish 1995). This tube widening by constraint release is analogous to that produced by the addition of a small-molecule solvent, and it is therefore called “dynamic dilution” (Ball and McLeish 1989). Dynamic dilution leads to much faster relaxation of segments near the branch point than would otherwise occur. When primitive-path fluctuations are analyzed along with “dynamic dilution,” the relaxation time of a tube segment a fraction x from the branch point changes from that of Eq. (3-65) to

$$\tau(x) = \tau_0 \exp \left[\frac{3M}{M_e} \left(\frac{(1-x)^2}{2} - \frac{(1-x)^3}{3} \right) \right] \quad (3-79)$$

The predictions of the storage and loss moduli that are obtained from these relaxation processes are in excellent agreement with experiment (see Fig. 3-38). The predicted exponential dependences of the longest relaxation time and zero-shear viscosity on the arm molecular weight are also well-confirmed experimentally (Pearson and Helfand 1984; Fetters et al. 1993), as is the insensitivity of these quantities to the number of arms at fixed

arm molecular weight. With recent improvements in the theory (Milner and McLeish 1997), superb agreement with experiment is obtained without adjustable parameters.

The nonlinear damping function, $h(\gamma)$, measured in step shearing on star polymers follows the Doi–Edwards prediction, just as $h(\gamma)$ does for linear polymers. Although one end of each arm of the star is anchored, the other end is free to retract, leading to the same strain softening as in linear polymers (Pearson 1987). Molecules with strands that are anchored at two ends, such as molecules with the topology of an “H,” a “comb,” or a gel fractal, are expected to show nonlinear behavior that is very different from that of stars (McLeish 1988a; Bick and McLeish 1996).

3.7.6.3 Melts with Irregular Long-Chain Branching

Some polymer melts, such as commercial low-density polyethylene, are not only poly-disperse, but also possess irregularly spaced long side branches. Here “long” means that the branches are longer than M_e , and hence are able to entangle with surrounding chains. Branches much shorter than this influence the friction coefficient but otherwise don’t affect reptation. The effects of long side branches on rheological properties are profound, and are difficult to consider theoretically, especially when compounded by irregularity in side-branch length and spacing along the backbone. In low-density polyethylene, the long side branches can themselves have long branches, thus forming tree-like structures (McLeish 1988b, 1995). Such structures are also present in partially *cross-linked* polymers, discussed in Chapter 5. Polymer strands that terminate in a branching point at one end but are free at the other cannot reptate, but they can still undergo retraction. The contributions of such a polymer strand to the *nonlinear* properties of the melt [i.e., to the strain-energy function $U(I_1, I_2)$] are expected to be similar to those of a freely reptating chain. The contribution to the linear properties [i.e., $G'(\omega)$ and $G''(\omega)$] are, however, greatly affected by the presence

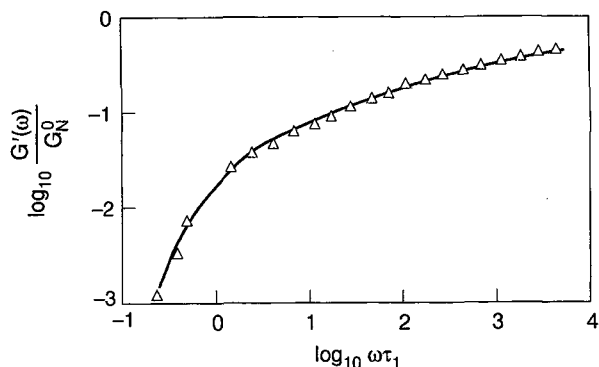


Figure 3.38 Reduced storage modulus G'/G_N^0 versus reduced frequency $\omega\tau_1$ for monodisperse star molecules, where G_N^0 is the plateau modulus for linear chains, and τ_1 is the terminal relaxation time of the star molecules. The symbols are experimental data for polyisoprene stars from Pearson and Helfand (1984), and the solid line is the prediction of the theory with primitive-path fluctuations and constraint release, with only τ_1 fitted (from Ball and McLeish 1989). (Reprinted with permission from Ball and McLeish, *Macromolecules* 22:1911 Copyright 1989, American Chemical Society.)

of a branch point at only one end of the chain, since one branch point is enough to suppress reptation so that relaxation must occur by primitive-path fluctuations.

Strands that terminate with a branch point at both of its ends can neither reptate nor completely retract. Relaxation of such strands presumably occurs by more complex, hierarchical processes discussed by McLeish (1988b). Here we simply note that the presence of branch points at both ends of a strand leads to *much more strain hardening* in extensional flows (Bishko et al. 1997; McLeish and Larson 1998). Low-density polyethylenes (LDPEs), which are highly branched, are well known for their extreme strain hardening behavior in extensional flows (Meissner 1972; Laun 1984) (see Fig. 3-39). The steady-state shear viscosity, as a function of shear rate, seems to be little affected by long-chain branching, however.

These characteristics of LDPEs, namely strain hardening in extension along with shear-thinning in shear, are highly desirable in some processing flows, such as film blowing. Film blowing is a process used to make thin polyethylene sheets for garbage bags, grocery wrappings, and so on, in which melt emerging from an annular die is blown up like a bubble by hot air directed along the die axis. The shear thinning of LDPE permits extrusion rates in the annular film-blowing die to be high, while the extension hardening helps stabilize the bubble (Minoshima and White 1986). New *metallocene* catalyst systems allow synthesis of polyethylenes with better controlled long-chain branching characteristics (Colvin 1997, *Chemical Week* 1997). Thus, to take advantage of these new capabilities, it is important that the effect of long-chain branches on rheology and polymer processing behavior be well understood.

Another interesting complication of long-chain branched polyethylenes, such as LDPE, is that time-temperature superposition fails. At high frequencies, their activation energy E_a is similar to that of unbranched or short-chain branched polyethylenes, such as high-density polyethylene (HDPE); but at low frequencies, long-branched polyethylenes (PEs) have activation energies that depend on molecular weight and can be up to 15 kcal/mol, more than twice as high as that of HDPE (Raju et al. 1979; Carella et al. 1986). This important phenomenon is not yet completely understood.

- Problem 3.12 and Worked Example 3.13 illustrate the usefulness of the methods discussed here for calculating flow properties of entangled branched and polydisperse polymers.

3.7.6.4 Semiempirical Constitutive Equations

The development of *molecular* constitutive equations for commercial melts is still a challenging unsolved problem in polymer rheology. Nevertheless, it has been found that for many melts, especially those without long-chain branching, the rheological behavior can be described by empirical or semiempirical constitutive equations, such as the separable K-BKZ equation, Eq. (3-72), discussed in Section 3.7.4.4 (Larson 1988). To use the separable K-BKZ equation, the memory function $m(t)$ and the strain-energy function U , or its strain derivatives $\partial U/\partial I_1$ and $\partial U/\partial I_2$, must be obtained empirically from rheological data.

Molecular polydispersity has a large effect on the memory function $m(t)$ and has a weak or modest effect on the strain-energy function $U(I_1, I_2)$ or, equivalently, on the

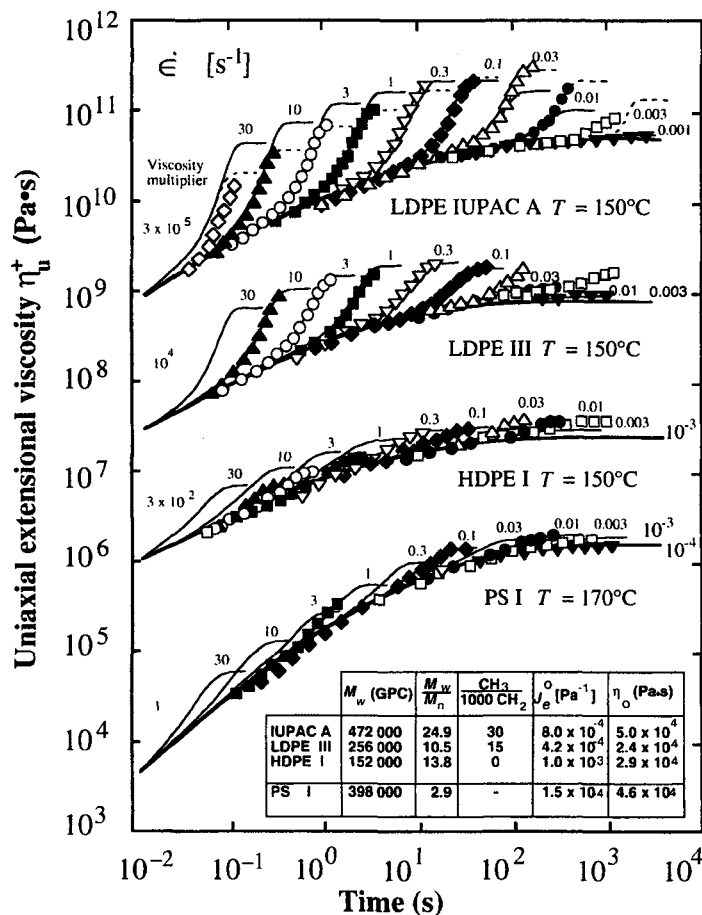


Figure 3.39 Uniaxial extensional viscosity $\bar{\eta}_u^+$ as a function of time following start-up of steady uniaxial extension at the extension rates $\dot{\epsilon}$ indicated. Data are shown for an unbranched polystyrene (PS I), a high-density polyethylene with short, unentangled side branches (HDPE I), and two low-density polyethylenes (LDPE III and IUPAC A), with long side branches. (From Laun 1984, with permission from the Universidad Nacional Autónoma de México.)

damping function (Osaki 1993). Long-chain side branching, which is present in LDPE, strongly affects the strain-energy function, making such melts less strain-softening than melts composed of only linear chains, especially in uniaxial and planar extensional flows (Larson 1988; Osaki 1993; McLeish and Larson 1998). Empirically, the linear memory function $m(t - t')$ can be obtained from linear viscoelastic testing, such as small-amplitude oscillatory shearing. The function U determines the nonlinear viscoelastic properties of the material and must be obtained by large-strain experiments, such as a series of step-strain experiments. Various empirical expressions for the strain-energy function $U(I_1, I_2)$, or for ϕ_1 and ϕ_2 , can be found in the literature (Wagner 1976; Wagner and Laun; 1978; Laun 1978; Larson 1988). Two of the most popular forms are

$$\phi_1 = f_1 e^{-n_1 \sqrt{I-3}} + f_2 e^{-n_2 \sqrt{I-3}}, \quad \phi_2 = 0$$

$$\text{with } I \equiv \alpha I_1 + (1 - \alpha) I_2 \quad (\text{Wagner et al. 1979})$$

and

$$\phi_1 = \frac{1}{a(I_1 - 3) + b(I_2 - 3)}, \quad \phi_2 = 0 \quad (\text{Papanastasiou et al. 1983})$$

[These forms are not “true” K–BKZ kernels, since they are not derived from a potential function $U(I_1, I_2)$.] Fits to shear and extensional flow data for “IUPAC A,” a well-studied LDPE, give $f_1 = 0.57$, $f_2 = 0.43$, $n_1 = 0.31$, $n_2 = 0.106$, and $\alpha = 0.032$ for the form proposed by Wagner et al. (1979), and $a = 0.0013$ and $b = 0.068$ for that of Papanastasiou et al. (1983).

While these functions have been adjusted to describe shear and uniaxial extensional flows, they seem to work poorly for *planar extension* of LDPE (Samurkas et al. 1989). Planar extensional flow represents a particularly difficult test for K–BKZ-type constitutive equations, since fits to shear data fix all the model parameters required for planar extension, and there is therefore no “wobble” room left to obtain a fit to the latter. (This is because $I_1 = I_2$ in both shear and planar extension.) A recent non-K–BKZ *molecular* constitutive equation derived from reptation-related ideas shows improved qualitative agreement with planar extensional data (McLeish and Larson 1998).

The K–BKZ and other integral constitutive equations discussed above can be regarded as generalizations of the Lodge integral, Eq. (3-24). The upper-convected Maxwell (UCM) equation, which is the differential equivalent of the one-relaxation-time Lodge equation, can also be generalized to make possible more realistic predictions of nonlinear phenomena. Many differential constitutive equations of the Maxwell type have been proposed; most of them are of the following form:

$$\overset{\nabla}{\sigma} + \frac{1}{\tau} \sigma + \mathbf{G}(\sigma, \mathbf{D}) + \mathbf{H}(\sigma) = 2\mathbf{G}\mathbf{D} \quad (3-80)$$

The stress tensor in this expression has been defined such that at equilibrium $\sigma = \mathbf{0}$, rather than $G\delta$. Some of the proposed possible forms for the functions $\mathbf{G}(\sigma, \mathbf{D})$ and $\mathbf{H}(\sigma)$ are

$$\mathbf{G} = \xi(\mathbf{D} \cdot \sigma + \sigma \cdot \mathbf{D}), \quad \mathbf{H} = \mathbf{0} \quad (\text{Johnson and Segalman 1977}) \quad (3-81a)$$

$$\mathbf{G} = \mathbf{0}, \quad \mathbf{H} = \alpha \frac{1}{\tau G} \sigma : \sigma \quad (\text{Giesekus 1966, 1982}) \quad (3-81b)$$

$$\mathbf{G} = \xi(\mathbf{D} \cdot \sigma + \sigma \cdot \mathbf{D}),$$

$$\mathbf{H} = \frac{1}{\tau} \left[\exp\left(\frac{\alpha}{G} \text{tr } \sigma\right) - 1 \right] \sigma \quad (\text{Phan-Thien and Tanner 1977, 1978}) \quad (3-81c)$$

$$\mathbf{G} = \frac{2}{3} \frac{\alpha}{G} \mathbf{D} : \sigma(\sigma + G\delta), \quad \mathbf{H} = \mathbf{0} \quad (\text{Larson 1984b}) \quad (3-81d)$$

$$\mathbf{G} = \alpha(2\mathbf{D} : \mathbf{D})^{1/2} \sigma, \quad \mathbf{H} = \mathbf{0} \quad (\text{White and Metzner 1963}) \quad (3-81e)$$

The notation “tr” stands for the trace of the tensor. These expressions contain parameters, such as ξ and α , that must be obtained by fits to nonlinear rheological data. None of

these equations fit time-dependent experimental data well unless a spectrum of relaxation modes is introduced in a way analogous to that described above for the UCM equation. That is, G , τ , and σ in Eqs. (3-80) and (3-81a)–(3-81e) must be subscripted with a mode index i ; and the total stress must be given by a sum of the stresses from all modes, as in Eq. (3-37). Comparisons of the predictions of the various equations to rheological data for melts are presented elsewhere (Larson 1988; Bird et al. 1987a, 1987b; Tanner 1985).

• Worked Example 3.14 and Problem 3.15 help you derive predictions from phenomenological constitutive equations.

3.8 SUMMARY

The steady-state and transient behavior of solutions of long polymer molecules that are dilute enough that coils only rarely overlap can be described by beads-and-springs models. In steady flows, the shear thinning and strong extension hardening of dilute solutions are predicted by simple finitely extensible dumbbell models. Time-dependent phenomena can in principle be predicted by using more complex models with multiple beads and springs, and with hydrodynamic interactions accounted for using the Zimm theory.

If the molecules are rather short ($M < M_c \approx 3M_e$), they remain unentangled even in the melt. In that case, the low flow-rate properties of the melt seem to be described by the simple Rouse theory, whose rheological predictions are similar to the dumbbell model. At flow rates or frequencies that are high compared to the inverse of the longest relaxation time, the rheological behavior of such melts is influenced by “glassy” relaxation modes, similar to those influencing the behavior of small-molecule glass-forming liquids discussed in Chapter 4.

Melts and dense solutions of long polymer molecules ($M \gg M_e$) are entangled, and they can in general be described by versions of the de Gennes’ reptation theory. Reptation theory assumes that long-range polymer motion occurs by a snake-like motion; thus, the gross molecular motion is confined to a tube that prohibits significant lateral motion. The escape from the tube is slow, leading at high molecular weights to a long plateau in the linear storage modulus, G' . Thus, for small deformations at frequencies in the plateau region, the material behaves almost elastically. If the sample is highly deformed, the tube is deformed, but a rapid retraction of the chain within it is permitted; this retraction accounts for the nonlinear strain softening in the shear modulus. Based on reptation and retraction, Doi and Edwards developed a constitutive model for concentrated solutions and melts. With some approximations, it reduces to a constitutive equation of K–BKZ class that requires only two parameters to define the linear viscoelastic response and none at all for the nonlinear response.

The Doi–Edwards model has been extended to allow processes of “primitive-path fluctuations,” “constraint release,” and “tube stretching.” These extensions of the theory allow accurate prediction of many steady-state and time-dependent phenomena, including shear thinning, stress overshoots, and so on. Predictions of strain localization and slip at walls

may in the future be possible using reptation ideas. The theory can be extended to account for the effects of simple branching and polydispersity. For complex commercial melts, however, it may be more convenient for some purposes to fit semiempirical constitutive equations, such as the K-BKZ equation or Maxwell-like differential equations, to experimental data.

REFERENCES

- Acierno D, Titomanlio G, Marrucci G (1974). *J Polym Sci Polym Phys Ed* 12:2177.
- Amelar S, Eastman CE, Morris RL, Smeltzly MA, Lodge TP, von Meerwall ED (1991). *Macromolecules* 24:3506.
- Archer LA, Chen Y-L, Larson RG (1995). *J Rheol* 39:519.
- Armstrong RC, Gupta SK, Basaran O (1980). *Polym Eng Sci* 20:466.
- Baird DG, Dimitris IC (1995). *Polymer Processing: Principles and Design*, Butterworths, London.
- Ball RC, McLeish TCB (1989). *Macromolecules* 22:1911.
- Bercea M, Peiti C, Simionescu B, Navard P (1993). *Macromolecules* 26:7095.
- Berker A, Chynoweth S, Klomp UC, Michopoulos Y (1992). *J Chem Soc Faraday Trans* 88:1719.
- Bernstein B, Kearsley EA, Zapas LJ (1963). *Trans Soc Rheol* 7:391.
- Berry GC, Fox TG (1968). *Adv Polym Sci* 5:261.
- Bianchi U, Peterlin A (1968). *J Polym Sci A-2* 6:1011.
- Bick DK, McLeish TCB (1996). *Phys Rev Lett* 76:2587.
- Bird RB, Armstrong RC, Hassager O (1977). *Dynamics of Polymeric Liquids*, Vol 1, 1st ed, Wiley, New York.
- Bird RB, Armstrong RC, Hassager O (1987a). *Dynamics of Polymeric Liquids*, Vol 1, 2nd ed, Wiley, New York.
- Bird RB, Curtiss CF, Armstrong RC, Hassager O (1987b). *Dynamics of Polymeric Liquids*, Vol 2, 2nd ed, Wiley, New York.
- Bishko G, McLeish TCB, Harlen O, Larson RG (1997). *Phys Rev Lett* 79:2352.
- Boger DV, Binnington R (1977). *Trans Soc Rheol* 22:515.
- Brochard F, de Gennes PG (1992). *Langmuir* 8:3033.
- Brown EF, Burghardt WR, Kahvand H, Venerus DC (1995). *Rheol Acta* 34:221.
- Byars JA, Öztekin A, Brown RA, McKinley GH (1994). *J Fluid Mech* 271:173.
- Carella JM, Gotro JT, Graessley WW (1986). *Macromolecules* 19:659.
- Cates ME, McLeish TCB, Marrucci G (1993). *Europhys Lett* 21:451.
- Cathey CA, Fuller GG (1990). *J Non-Newton Fluid Mech* 34:63.
- Chemical Week* (1997). May 21:23.
- Colvin R (1997). *Mod Plastics*, May:62.
- Cottrell FR, Merrill EQ, Smith KA (1969). *J Polym Sci A-2* 7:1415.
- Currie PK (1980). In *Rheology, Proceedings of the Eighth International Congress on Rheology*, Naples, Italy.
- Decruppe JP, Cressely R, Makhloufi R, Cappelaere E (1995). *Colloid Polym Sci* 273:346.
- de Gennes PG (1971). *J Chem Phys* 55:572.
- de Gennes PG (1974). *J Chem Phys* 60:5030.
- de Gennes PG (1975). *J Phys (Paris)* 36:1199.
- de Gennes PG (1979). *Scaling Concepts in Polymer Physics*, Cornell University Press, Ithaca, New York.

- Dealy JM, Wissbrun KF (1990). *Melt Rheology and Its Role in Plastics Processing*, Van Nostrand Reinhold, New York.
- des Cloizeaux J (1988). *J Europhys Lett* 5:437; 6:475.
- Doi M, Edwards SF (1978a). *J Chem Soc Faraday Trans II* 74:1789, 1802, 1818.
- Doi M, Edwards SF (1978b). *J Chem Soc Faraday Trans II* 74:560, 918.
- Doi M, Edwards SF (1979). *J Chem Soc Faraday Trans II* 75:38, 918.
- Doi M, Edwards SF (1986). *The Theory of Polymer Dynamics*, Oxford University Press, New York.
- Doi M, Kuzuu NY (1980). *J Polym Sci Polym Lett Ed* 18:775.
- Doyle PS, Shaqfeh ESG, Gast AP (1997). *J Fluid Mech* 334:251.
- Doyle PS, Shaqfeh ESG, McKinley GH, Spiegelberg SH (1998). *J Fluid Mech*, submitted.
- Dünweg B, Kremer K (1991). *Phys Rev Lett* 66:2996.
- Edwards SF (1967). *Proc Phys Soc* 92:9.
- Einaga Y, Osaki K, Kurata M, Kimura S, Tamura M (1971). *Polym J* 2:550.
- Ferry JD (1980). *Viscoelastic Properties of Polymers*, 3rd ed, Wiley, New York.
- Fetters LJ, Kiss AD, Pearson DS, Quack GF, Vitis FJ (1993). *Macromolecules* 26:647.
- Fetters LJ, Lohse DJ, Richter D, Witten TA, Zirkel A (1994). *Macromolecules* 27:4639.
- Fixman M (1966). *J Chem Phys* 45:785; 793.
- Flory PJ (1953). *Principles of Polymer Chemistry*, Cornell University Press, Ithaca, NY.
- Flory PJ (1969). *Statistical Mechanics of Chain Molecules*, Wiley, New York, p 40.
- Flory PJ, Rehner J (1943). *J Chem Phys* 11:512.
- Fukuda M, Osaki K, Kurata M (1975). *J Polym Sci Polym Phys Ed* 13:1563.
- Fuller GG (1995). *Optical Rheometry of Complex Fluids*, Oxford University Press, New York.
- Fuller GG, Leal LG (1980). *Rheol Acta* 19:580.
- Fuller GG, Leal LG (1981). *J Non-Newt Fluid Mech* 8:271.
- Gao J, Weiner JH (1992). *Macromolecules* 25:3462.
- Gao J, Weiner JH (1994). *Macromolecules* 27:1201.
- Giesekus H (1962). *Rheol Acta* 2:50.
- Giesekus H (1966). *Rheol Acta* 5:29.
- Giesekus H (1982). *J Non-Newt Fluid Mech* 11:69.
- Graessley WW (1982). *Adv Polym Sci* 47:68.
- Green MS, Tobolsky AV (1946). *J Chem Phys* 14:80.
- Hall CK, Helfand E (1982). *J Chem Phys* 77:3275.
- Helfand E, Wasserman ZR, Weber TA (1980). *Macromolecules* 13:526.
- Hinch EJ (1974). In *Proceedings of the Symposium on Polymer Lubrication*, Brest.
- Hinch EJ (1994). *J Non-Newt Fluid Mech* 54:209.
- Horn A, Merrill EW (1984). *Nature* 312:140.
- Inoue T, Okamoto H, Osaki K (1991). *Macromolecules* 24:5670.
- Inoue T, Hwang EJ, Osaki K (1992). *J Rheol* 36:1737.
- James HM, Guth E (1943). *J Chem Phys* 11:455.
- Janeschitz-Kriegl H (1983). *Polymer Melt Rheology and Flow Birefringence*, Springer-Verlag, New York.
- Johnson RM, Schrag JL, Ferry JD (1970). *Polym J* 1:742.
- Johnson MW Jr, Segalman D (1977). *J Non-Newt Fluid Mech* 2:225.
- Kannan RM, Kornfield JA (1994). *J Rheol* 38:1127.
- Kausch HH (1985). *Colloid Polym Sci* 263:306.
- Kaye A (1962). College of Aeronautics, Cranford, UK, Note No 134.
- Keentok M, Georgescu AG, Sherwood AA, Tanner RI (1980). *J Non-Newt Fluid Mech* 6:303.

- Keller A, Odell JA (1985). *Colloid Polym Sci* 263:181.
- Keunings R (1997). *J Non-Newton Fluid Mech* 68:85.
- Kirkwood JG, Riseman J (1948). *J Chem Phys* 16:565.
- Kishbaugh AJ, McHugh AJ (1990). *J Non-Newton Fluid Mech* 34:181.
- Kolkka RW, Malkus DS, Rose TR (1991). *Rheol Acta* 30:430.
- Kotaka T, Suzuki H, Inagaki H (1966). *J Chem Phys* 45:2770.
- Kremer K, Grest GS (1990). *J Chem Phys* 92:5057.
- Kröger M, Loose W, Hess S (1993). *J Rheol* 37:1057.
- Kröger M (1995). *Rheology* 95(5):66.
- Kuhn W (1934). *Kolloid-Z* 68:2.
- Kuhn W, Grün F (1942). *Kolloid Z* 101:248.
- Landry CJ (1985). PhD Thesis, University of Wisconsin.
- Larson RG (1984a). In *Rheology, Proceedings of the Ninth International Congress on Rheology*, Acapulco, Mexico.
- Larson RG (1984b). *J Rheol* 28:545.
- Larson RG (1988). *Constitutive Equations for Polymer Melts and Solutions*, Butterworths, London.
- Larson RG (1990). *Rheol Acta* 29:371.
- Larson RG, Khan SA, Raju VR (1988). *J Rheol* 32:145.
- Larson RG, Goyal S, Aloisio C (1996). *Rheol Acta* 35:252.
- Larson RG, Mead DW, Doi M (1998). *Macromolecules*, in press.
- Larson RG, Perkins TT, Smith DE, Chu S (1997). *Phys Rev E* 55:1794.
- Larson RG (1998). *J Rheol*, submitted.
- Laun HM (1978). *Rheol Acta* 17:1.
- Laun HM (1984). In *Proceedings of the Ninth International Congress on Rheology*, Acapulco, Mexico.
- Lee EC, Solomon MJ, Muller SJ (1997). *Macromolecules*, 30:7313.
- Lin Y-H (1984). *J Rheol* 28:1.
- Lin Y-H (1987). *Macromolecules* 20:3080.
- Link A, Springer J (1993). *Macromolecules* 26:464.
- Lodge AS (1956). *Trans Faraday Soc* 52:120.
- Lodge AS (1968). *Rheol Acta* 7:379.
- Lodge AS (1989). *J Rheol* 33:821.
- Lodge AS, Wu Y (1972). University of Wisconsin Rheology Research Center Report No 19.
- Lodge TP (1993). *J Phys Chem* 97:1480.
- Lodge TP, Miller JW, Schrag JL (1982). *J Polym Sci: Polym Phys Ed* 20:1409.
- Lodge TP, Rotstein NA, Prager S (1990). *Adv Chem Phys* 79:1.
- Mackay ME, Boger DV (1987). *J Non-Newton Fluid Mech* 22:235.
- Macosko CW (1994). *Rheology Principles, Measurements, and Applications*, VCH Publishers, New York.
- Magda JJ, Larson RG, Mackay ME, (1988). *J Chem Phys* 89:2504.
- Magda JJ, Lee C-S, Muller SJ, Larson RG (1993). *Macromolecules* 26:1696.
- Man V (1984). PhD Thesis, University of Wisconsin.
- Marko JF, Siggia ED (1995). *Macromolecules* 28:8759.
- Marrucci G (1984). In *Advances in Transport Process*, Vol V, Mujamdar AS, Mashelkar RA (eds), Wiley, New York.
- Marrucci G (1996). *J Non-Newton Fluid Mech* 62:279.
- Marrucci G, Grizzuti N (1983). *J Rheol* 27:433.
- Marrucci G, Grizzuti N (1988). *Gazz Chim Ital* 118:179.

- Marrucci G, Ianniruberto G (1997). *Macromol Symp* 117:233.
- Massa DJ, Schrag JL, Ferry JD (1971). *Macromolecules* 4:210.
- McKinley GH (1996). Private communication.
- McLeish TCB (1987). *J Polym Sci Polym Phys Ed* 25:223.
- McLeish TCB (1988a). *Macromolecules* 21:1062.
- McLeish TCB (1988b). *Europhys Lett* 6:511.
- McLeish TCB (1995). *Physics World* March:32.
- McLeish TCB, Ball RC (1986). *J Polym Sci Polym Phys Ed* 24:1735.
- McLeish TCB, Larson RG (1998). *J Rheol*, 42:81.
- Mead DW (1994). *J Rheol* 38:1797.
- Mead DW (1996). *J Rheol* 40:633.
- Mead DW, Leal LG (1995). *Rheol Acta* 34:339.
- Meissner J (1972). *J Appl Polym Sci* 16:2877.
- Menasveta MJ, Hoagland DA (1991). *Macromolecules* 24:3427.
- Menezes EV, Graessley WW (1980). *Rheol Acta* 19:38.
- Menezes EV, Graessley WW (1982). *J Polym Sci Polym Phys Ed* 20:1817.
- Migler KB, Hervet H, Leger L (1993). *Phys Rev Lett* 70:287.
- Milner ST (1996). *J Rheol* 40:303.
- Milner ST, McLeish TCB (1997). *Macromolecules* 30:2159.
- Milner ST, McLeish TCB (1998). *Phys Rev Lett*, submitted.
- Minoshima W, White J (1986). *J Non-Newt Fluid Mech* 19:275.
- Montfort JP, Marin G, Monge P (1986). *Macromolecules* 19:393.
- Morawetz H (1979). *Science* 203:405.
- Morris RL, Amelar S, Lodge TP (1988). *J Chem Phys* 89:6523.
- Morrison FA, Larson RG (1992). *J Polym Sci Polym Phys Ed* 30:943.
- Muller R, Froelich D (1985). *Polymer* 26:1477.
- Muller SJ, Shaqfeh ESG, Larson RG (1993). *J Non-Newt Fluid Mech* 46:315.
- Nguyêñ H and Boger DV (1979). *J Non-Newt Fluid Mech* 5:353.
- Noda I, Yamada Y, Nagasawa M (1968). *J Phys Chem* 72:2890.
- Onogi S, Masuda T, Kitagawa K (1970). *Macromolecules* 3:109.
- Osaki K (1993). *Rheol Acta* 32:429.
- Osaki K, Fukuda M, Kurata M (1975). *J Polym Sci Polym Phys Ed* 13:775.
- Osaki K, Kimura S, Kurata M (1981). *J Polym Sci Polym Phys Ed* 19:517.
- Osaki K, Okamoto H, Inoue T, Hwang E-J (1995). *Macromolecules* 28:3635.
- Oseen CW (1910). *Arf Mat Astr Fys* 6(29):1.
- Öttinger HC (1985). *J Chem Phys* 83:6535.
- Öttinger HC (1986). *J Chem Phys* 84:4068.
- Öttinger HC (1987). *J Chem Phys* 86:3731.
- Papanastasiou AC, Scriven LE, Macosko CW (1983). *J Rheol* 27:387.
- Pearson DS (1987). *Rubber Chem Technol*, Rubber Reviews.
- Pearson DS, Helfand E (1984). *Macromolecules* 17:888.
- Pearson DS, Kiss AD, Fetters LJ, Doi M (1989). *J Rheol* 33:517.
- Pearson DS, Herbolzheimer E, Grizzuti N, Marrucci G (1991). *J Polym Sci B Polym Phys Ed* 29:1589.
- Perkins TT, Smith DE, Chu S (1994a). *Science* 264:819.
- Perkins TT, Smith DE, Chu S (1994b). *Science* 264:822.
- Perkins TT, Smith DE, Larson RG, Chu S (1995). *Science* 268:83.
- Perkins TT, Smith DE, Chu S (1997). *Science* 276:2016.
- Peterlin A (1960). *J Chem Phys* 33:1799.
- Peterlin A (1961). *Makromol Chem.* 44:338.

- Phan-Thien N, Tanner RI (1977). *J Non-Newt Fluid Mech* 2:353.
- Phan-Thien N, Tanner RI (1978). *J Rheol* 22:259.
- Pierleoni C, Ryckaert J-P (1991). *Phys Rev Lett* 66:2992.
- Plazek DJ (1965). *J Phys Chem.* 69:3480.
- Rabin Y (1987). *J Chem Phys* 86:5215.
- Raju VR, Rachapudy H, Graessley WW (1979). *J Polym Sci Polym Phys Ed* 17:1223.
- Richter D, Butera R, Fetters LJ, Huang JS, Farago B, Ewen B (1992). *Macromolecules* 25:6156.
- Ronca GJ (1983). *J Chem Phys* 79:1031.
- Rouse PE Jr (1953). *J Chem Phys* 21:1272.
- Rubinstein M, Helfand E, Pearson DS (1987). *Macromolecules* 20:822.
- Russell, TP, Deline VR, Dozier WD, Felcher GP, Agrawal G, Wool RP, Mays JW (1993). *Nature* 365:235.
- Ryskin G (1987). *J Fluid Mech* 178:423.
- Sahouani H, Lodge TP (1992). *Macromolecules* 25:5632.
- Sammler RL, Landry CJT, Woltman GR, Schrag JL (1990). *Macromolecules* 23:2388.
- Samurkas T, Larson RG, Dealy JM (1989). *J Rheol* 33:559.
- Smith SB, Finzi L, Bustamante C (1992). *Science* 258:1122.
- Sridhar T, Gupta RK, Boger DV, Binnington R (1986). *J Non-Newt Fluid Mech* 21:115.
- Talbott WH, Goddard JD (1979). *Rheol Acta* 18:507.
- Tanner RI (1985). *Engineering Rheology*, Oxford University Press, New York.
- Tirrell M (1984). *Rubber Chem Technol* 57:523.
- Tirtaatmadja V, Sridhar T (1993). *J Rheol* 37:1081.
- Treloar LRG (1943). *Trans Faraday Soc* 37:36; 241.
- Treloar LRG (1975). *The Physics of Rubber Elasticity*, 3rd ed, Clarendon Press, Oxford.
- Tsenoglou C (1987). *ACS Polym Preprints* 28:185.
- Tuminello WH (1986). *Polym Eng Sci* 26:1339.
- Urakawa O, Takahashi M, Masuda T, Golshan Ebrahimi N (1995). *Macromolecules* 28:7196.
- Verhoef MRJ, van den Brule BHAA, Hulsen MA (1997). *J Non-Newt Fluid Mech*, submitted.
- Viovy JL, Rubinstein M, Colby RH (1991). *Macromolecules* 24:3587.
- Vrentas CM, Graessley WW (1982). *J Rheol* 26:359.
- Wagner MH (1976). *Rheol Acta* 15:136.
- Wagner MH, Laun HM (1978). *Rheol Acta* 17:138.
- Wagner MH, Raible T, Meissner J (1979). *Rheol Acta* 18:427.
- Wales JLS (1976). *The Application of Flow Birefringence to Rheological Studies of Polymer Melts*, Delft University Press, Delft, Holland.
- Wall FT (1942). *J Chem Phys* 10:485.
- Warner HR Jr (1972). *I&EC Fundam* 11:379.
- Wasserman SH, Graessley WW (1992). *J Rheol* 36:543.
- Weber TA, Helfand E (1983). *J Phys Chem* 87:2881.
- White JL, Metzner AB (1963). *J Appl Polym Sci* 8:1367.
- Williams ML, Landel RF, Ferry JD (1955). *J Am Chem Soc* 77:3701.
- Yamamoto M (1956). *J Phys Soc Jpn* 11:413.
- Yamamoto M (1957). *J Phys Soc Jpn* 12:1148.
- Yamamoto M (1958). *J Phys Soc Jpn* 13:1200.
- Ylitalo CM, Fuller GG, Abetz V, Stadler R, Pearson DS (1990). *Rheol Acta* 29:543.
- Zawada JA, Fuller GG, Colby RH, Fetters LJ, Roovers J (1994). *Macromolecules* 27:6851.
- Zhu W, Ediger MD (1995). *Macromolecules* 28:7549.
- Zhu W, Ediger MD (1997). *Macromolecules* 30:1205.
- Zimm BH (1956). *J Chem Phys* 24:269.
- Zylka W, Öttinger HC (1989). *J Chem Phys* 90:474.

PROBLEMS AND WORKED EXAMPLES

Problem-3.1 (Worked Example)

From Eq. (3-24) for a “rubber-like liquid,” assuming a single relaxation time τ and modulus G , calculate formulas for the extensional viscosity as a function of time after start-up of steady uniaxial extension at extension rate $\dot{\epsilon}$.

ANSWER:

For a steady uniaxial extensional flow, the velocity gradient tensor is given by Eq. (1-9):

$$\nabla \mathbf{v} = \begin{pmatrix} \dot{\epsilon} & 0 & 0 \\ 0 & -\dot{\epsilon}/2 & 0 \\ 0 & 0 & -\dot{\epsilon}/2 \end{pmatrix} \quad (\text{A3-1})$$

The Finger deformation tensor for this flow is obtained from Eq. (1-19) with $\lambda_2 = \lambda_3 = \lambda_1^{-1/2}$. Hence, taking $\lambda \equiv \lambda_1$, we obtain

$$\mathbf{B} = \begin{pmatrix} \lambda^2 & 0 & 0 \\ 0 & \lambda^{-1} & 0 \\ 0 & 0 & \lambda^{-1} \end{pmatrix} \quad (\text{A3-2})$$

where $\lambda = \lambda(t', t)$ is the stretch ratio in the direction of uniaxial stretch between times t' and t .

Suppose the sample is completely relaxed in a state of equilibrium until time 0, and then an extensional flow with extension rate $\dot{\epsilon}$ begins at time 0. The stretch ratio history in this case is given by

$$\lambda(t', t) = \begin{cases} \exp[\dot{\epsilon}(t - t')] & \text{for } t' > 0 \\ \exp(\dot{\epsilon}t) & \text{for } t' \leq 0 \end{cases} \quad (\text{A3-3})$$

Note that for $t' < 0$, $\lambda(t', t) = \exp(\dot{\epsilon}t)$ is independent of t' , since the sample is not being stretched at times less than 0. From Eq. (A3-2), we obtain the components of the Finger tensor:

$$B_{11}(t', t) = \begin{cases} \exp[2\dot{\epsilon}(t - t')] & \text{for } t' > 0 \\ \exp(2\dot{\epsilon}t) & \text{for } t' \leq 0 \end{cases} \quad (\text{A3-4})$$

$$B_{22}(t', t) = B_{33}(t', t) = \begin{cases} \exp[-\dot{\epsilon}(t - t')] & \text{for } t' > 0 \\ \exp(-\dot{\epsilon}t) & \text{for } t' \leq 0 \end{cases} \quad (\text{A3-5})$$

We now wish to solve Eq. (3-24), the equation for a “rubber-like liquid”:

$$\boldsymbol{\sigma} = \int_{-\infty}^t m(t - t') \mathbf{B}(t', t) dt' \quad (\text{A3-6})$$

where we consider a single relaxation time so that $m(t - t') \equiv (G/\tau) \exp[(t' - t)/\tau]$. To compute the stress component σ_{11} , we insert Eq. (A3-4) into the “11” component of Eq. (A3-6); we must break the integral into two pieces:

$$\sigma_{11} = \int_{-\infty}^0 \frac{G}{\tau} e^{(t'-t)/\tau} e^{2\dot{\epsilon}t} dt' + \int_0^t \frac{G}{\tau} e^{(t'-t)/\tau} e^{2\dot{\epsilon}(t-t')} dt' \quad (\text{A3-7})$$

Likewise, the “22” component of Eq. (A3-6) yields

$$\sigma_{22} = \int_{-\infty}^0 \frac{G}{\tau} e^{(t'-t)/\tau} e^{-\dot{\epsilon}t} dt' + \int_0^t \frac{G}{\tau} e^{(t'-t)/\tau} e^{-\dot{\epsilon}(t-t')} dt' \quad (\text{A3-8})$$

Carrying out these integrations gives

$$\sigma_{11} = G e^{-(1-2\dot{\epsilon}\tau)t/\tau} + \frac{G}{1-2\dot{\epsilon}\tau} [1 - e^{-(1-2\dot{\epsilon}\tau)t/\tau}] \quad (\text{A3-9})$$

$$\sigma_{22} = G e^{-(1+\dot{\epsilon}\tau)t/\tau} + \frac{G}{1+\dot{\epsilon}\tau} [1 - e^{-(1+\dot{\epsilon}\tau)t/\tau}] \quad (\text{A3-10})$$

Note that if $\dot{\epsilon} > 1/(2\tau)$, σ_{11} diverges exponentially as time increases. If, however, $\dot{\epsilon} < 1/(2\tau)$, a steady-state is reached in which

$$\sigma_{11} = \frac{G}{1-2\dot{\epsilon}\tau}, \quad \sigma_{22} = \frac{G}{1+\dot{\epsilon}\tau} \quad (\text{A3-11})$$

The steady-state uniaxial extensional viscosity $\bar{\eta}_u$ is given by $(\sigma_{11} - \sigma_{22})/\dot{\epsilon}$. Note that in the limit of small $\dot{\epsilon}$, $\bar{\eta}_u$ approaches the Trouton limit, $\bar{\eta}_u \rightarrow 3G\tau$.

Problem 3.2 (Worked Example)

From Eq. (3-32) for a dilute solution of Hookean elastic dumbbells with relaxation time τ and modulus G , calculate polymer contributions to the extensional viscosity as a function of time after start-up of steady extension at extension rate $\dot{\epsilon}$.

ANSWER:

Equation (3-32) is

$$\overset{\nabla}{\sigma}^p + \frac{1}{\tau} (\sigma^p - G\delta) = \mathbf{0} \quad (\text{A3-12})$$

where the “ ∇ ” above σ^p is the upper-convected time derivative, defined in Eq. (3-33). Using this definition, we get Eq. (3-30):

$$\dot{\sigma}^p - \nabla \mathbf{v}^T \cdot \sigma^p - \sigma^p \cdot \nabla \mathbf{v} + \frac{1}{\tau} (\sigma^p - G\delta) = \mathbf{0} \quad (\text{A3-13})$$

Note first that if the fluid is at a state of equilibrium with no flow, then the time derivative $\dot{\sigma}^p$ is equal to zero, and the velocity gradient $\nabla \mathbf{v}$ is also zero. This implies from the above equations that $\sigma^p = G\delta$. Hence $\sigma_{11}^p = \sigma_{22}^p = \sigma_{33}^p = G$ at equilibrium, and $\sigma_{ij}^p = 0$, for $i \neq j$. Thus, although the diagonal stress components are not zero at equilibrium, they are all equal to each other, and *the nondiagonal components are all equal to zero*. Hence, the stress tensor is *isotropic*, but nonzero at equilibrium. (If one redefines the stress tensor as $\Sigma^p \equiv \sigma^p - G\delta$, then $\Sigma^p = \mathbf{0}$ at equilibrium. The upper-convected Maxwell equation can then be rewritten in terms of Σ^p .)

For a steady uniaxial extensional flow, we can assume by symmetry that the stress tensor contains only diagonal components. We can then evaluate the terms in Eq. (A3-13) containing the velocity gradient by using Eq. (A3-1):

$$(\nabla \mathbf{v})^T \cdot \sigma^p = \begin{pmatrix} \dot{\epsilon} & 0 & 0 \\ 0 & -\dot{\epsilon}/2 & 0 \\ 0 & 0 & -\dot{\epsilon}/2 \end{pmatrix} \cdot \begin{pmatrix} \sigma_{11} & 0 & 0 \\ 0 & \sigma_{22} & 0 \\ 0 & 0 & \sigma_{33} \end{pmatrix}$$

$$= \begin{pmatrix} \sigma_{11}^p \dot{\epsilon} & 0 & 0 \\ 0 & \frac{-\sigma_{22}^p \dot{\epsilon}}{2} & 0 \\ 0 & 0 & \frac{-\sigma_{33}^p \dot{\epsilon}}{2} \end{pmatrix} \quad (\text{A3-14})$$

Since $\nabla \mathbf{v}$ is a diagonal tensor, and hence symmetric, the term $\boldsymbol{\sigma}^p \cdot \nabla \mathbf{v}$ equals $\nabla \mathbf{v}^T \cdot \boldsymbol{\sigma}^p$. Thus, for a steady uniaxial extensional flow, Eq. (A3-13) can be written as

$$\begin{pmatrix} \dot{\sigma}_{11}^p & 0 & 0 \\ 0 & \dot{\sigma}_{22}^p & 0 \\ 0 & 0 & \dot{\sigma}_{33}^p \end{pmatrix} - \begin{pmatrix} 2\sigma_{11}^p \dot{\epsilon} & 0 & 0 \\ 0 & -\sigma_{22}^p \dot{\epsilon} & 0 \\ 0 & 0 & -\sigma_{33}^p \dot{\epsilon} \end{pmatrix} + \frac{1}{\tau} \begin{pmatrix} \sigma_{11}^p - G & 0 & 0 \\ 0 & \sigma_{22}^p - G & 0 \\ 0 & 0 & \sigma_{33}^p - G \end{pmatrix} = \begin{pmatrix} 0 & 0 & 0 \\ 0 & 0 & 0 \\ 0 & 0 & 0 \end{pmatrix} \quad (\text{A3-15})$$

This tensor equation can be broken down into three scalar equations:

$$\dot{\sigma}_{11}^p - 2\dot{\epsilon}\sigma_{11}^p + \frac{1}{\tau}(\sigma_{11}^p - G) = 0 \quad (\text{A3-16})$$

$$\dot{\sigma}_{22}^p + \dot{\epsilon}\sigma_{22}^p + \frac{1}{\tau}(\sigma_{22}^p - G) = 0 \quad (\text{A3-17})$$

$$\dot{\sigma}_{33}^p + \dot{\epsilon}\sigma_{33}^p + \frac{1}{\tau}(\sigma_{33}^p - G) = 0 \quad (\text{A3-18})$$

These can be solved once an initial condition is specified. If the fluid is initially at equilibrium and we turn on the steady extensional flow at time 0, we have the initial conditions $\sigma_{11}^p(0) = \sigma_{22}^p(0) = \sigma_{33}^p(0) = G$. Then, rewriting Eq. (A3-16), we obtain

$$e^{(2\dot{\epsilon}-1/\tau)t} \frac{d}{dt} (e^{-(2\dot{\epsilon}-1/\tau)t} \sigma_{11}^p) = \frac{G}{\tau} \quad (\text{A3-19})$$

Multiplying through by $\exp[-(2\dot{\epsilon} - 1/\tau)t]$ and integrating gives

$$\begin{aligned} & e^{-(2\dot{\epsilon}\tau-1)t/\tau} \sigma_{11}^p(t) - \sigma_{11}^p(0) \\ &= \frac{G}{\tau} \int_0^t e^{-(2\dot{\epsilon}\tau-1)t'/\tau} dt' = -\frac{G}{2\dot{\epsilon}\tau-1} [e^{-(2\dot{\epsilon}\tau-1)t/\tau} - 1] \end{aligned} \quad (\text{A3-20})$$

where $\sigma_{11}^p(0) = G$. We can then multiply through by $\exp[(2\dot{\epsilon}\tau - 1)t/\tau]$ and rearrange to obtain

$$\sigma_{11}^p(t) = G e^{-(1-2\dot{\epsilon}\tau)t/\tau} + \frac{G}{1-2\dot{\epsilon}\tau} [1 - e^{-(1-2\dot{\epsilon}\tau)t/\tau}] \quad (\text{A3-21})$$

Similarly, we obtain for the other two stress components:

$$\sigma_{22}^p(t) = \sigma_{33}^p(t) = G e^{-(1+\dot{\epsilon}\tau)t/\tau} + \frac{G}{1+\dot{\epsilon}\tau} [1 - e^{-(1+\dot{\epsilon}\tau)t/\tau}] \quad (\text{A3-22})$$

Note that these stresses are *identical* to those obtained with the integral equations, Eqs. (A3-9) and (A3-10).

We leave it as an exercise for the reader to derive the corresponding equations for the shear stress and normal stresses in start-up of steady shearing, using both the integral and differential equations.

Problem 3.3 From Eq. (3-4), estimate the “overlap concentration” in g/cm^3 for polystyrene of molecular weight 10^7 daltons in a theta solvent. Compare this to the value obtained from Eq. (3-8), where the intrinsic viscosity for a theta solvent is given by $[\eta]_0 = K_\theta M^{1/2}$, with K_θ given by Eq. (3-49).

Problem 3.4(a) (Worked Example) Suppose you want to estimate the viscosity of a very viscous colloidal gel, at 25°C . You pour the unaggregated liquid dispersion, or “sol,” into a spherical mold, add a bit of acid, and voilà!, it gels in a minute or so. Now you carefully remove the gel from the mold; it is a 10-cm-diameter spherical ball. You place this ball on a flat surface in a humidity chamber at 25°C so that the gel does not dry out. After 1000 hours, you find that the gel has sagged so that its height has decreased to 90% of the original height. By using dimensional analysis and assuming that at the slow rate of sagging the gel is Newtonian, determine the scaling law showing how the time T to sag a given amount scales with sphere radius R , gel viscosity η , gel density ρ , and gravitational constant g . You do not need to derive an exact formula, only a law of proportionality.

ANSWER:

Consider the momentum and mass balance equations in the absence of inertia for an incompressible material:

$$-\nabla p + \nabla \cdot \boldsymbol{\sigma} = \rho g \mathbf{e}_z, \quad \nabla \cdot \mathbf{v} = 0 \quad (\text{A3-23})$$

where \mathbf{e}_z is the downward-pointing unit vector. The gel is a very viscous, yet Newtonian, liquid at the conditions of the experiment. Hence, $\nabla \cdot \boldsymbol{\sigma} = \eta \nabla^2 \mathbf{v}$. The momentum balance equation then becomes

$$-\nabla p + \eta \nabla^2 \mathbf{v} = \rho g \mathbf{e}_z \quad (\text{A3-24})$$

Now, we perform a dimensional analysis. Let t be the time for the gel to sag 10%. Let all quantities superscripted by an asterisk be dimensionless. The velocity \mathbf{v} , gradient operator ∇ , and pressure p can then be rescaled as

$$\mathbf{v} = \frac{R}{t} \mathbf{v}^*, \quad \nabla = \frac{1}{R} \nabla^*, \quad p = \frac{\eta}{t} p^* \quad (\text{A3-25})$$

Then we can rewrite Eq. (A3-24) as

$$-\left(\frac{\eta}{tR}\right) \nabla^* p^* + \left(\frac{\eta}{tR}\right) \nabla^{*2} \mathbf{v}^* = \rho g \mathbf{e}_z$$

Multiplying through by tR/η gives

$$-\nabla^* p^* + \nabla^{*2} \mathbf{v}^* = \frac{tR\rho g}{\eta} \mathbf{e}_z \quad (\text{A3-26})$$

The boundary conditions are zero stress at the gel surfaces that contact air (we neglect surface tension) and zero velocity at the surfaces that contact the flat solid surface. Thus all boundary conditions can be written so that the right sides are zero, and they rescale trivially. Likewise, the mass balance equation in Eq. (A3-23) rescales trivially.

Equation (A3-26) along with the mass balance equation and the boundary conditions form a linear problem which has a unique solution for each value of the coefficient $tR\rho g/\eta$. The same solution is therefore obtained if two or more constants in the coefficient $tR\rho g/\eta$ are varied in off-setting ways so that $tR\rho g/\eta$ remains constant. Hence, it follows that the sag time t must obey

$$t \propto \frac{\eta}{R\rho g} \quad (\text{A3-27})$$

Problem 3.4(b) (Worked Example) Suppose you now mold a 1-cm-diameter spherical ball of 1,4-polyisoprene and place it on a flat surface at 25°C and find that the time for it to sag to 90% of its original height is 10 minutes. Now you place the polyisoprene in a rheometer at 25°C to measure its viscosity, but the viscosity is too high to measure accurately, so you raise the temperature to 100°C and measure a zero-shear viscosity of 10⁵ P. Use this information and that in Problem 3.4(a) to determine the viscosity of the gel in Problem 3.4(a), given that the gel density is $\rho_{\text{gel}} = 3\text{g/cm}^3$.

ANSWER:

From Table 3-3, the polyisoprene density is $\rho_{\text{pi}} = 0.830\text{g/cm}^3$, and the viscoelastic shift factor obeys the WLF relationship

$$\log_{10} a_T = -\frac{c_1^0(T - T_0)}{(T - T_\infty)} \quad (\text{A3-28})$$

where for 1,4-polyisoprene $c_1^0 = 8.86$, $T_\infty = 146\text{K}$, T_0 is the reference temperature (at which we take a_T to be unity), and T is the temperature at which the rheological properties are measured. We can choose T_0 to be the temperature of the sag experiments, T_0 to be 298 K, and T to be the temperature at which the viscosity of the polyisoprene is measured. According to Eq. (A3-28), we have

$$\log_{10} a_T = -\frac{8.86(373 - 298)}{373 - 146} = -2.93$$

Therefore, $a_T = 0.0012$. This means that the longest relaxation time τ of the polyisoprene at 100°C is 0.0012 times its value at 25°C. The viscosity η changes roughly in proportion to the relaxation time, if the small vertical shift factor is neglected. Thus,

$$\frac{\eta(25^\circ\text{C})}{\eta(100^\circ\text{C})} \approx \frac{\tau(25^\circ\text{C})}{\tau(100^\circ\text{C})} = \frac{1}{a_T} = 846$$

Because η for polyisoprene at 100°C is 10⁵ P, we find that η at 25°C is 8.46×10^7 P.

Since the time for the gel to sag 10% at 25°C is 1000 hours, we can use the scaling law in Eq. (A3-27) to obtain

$$(\text{time for gel to sag } 10\%) = \left(\frac{R_{\text{pi}}}{R_{\text{gel}}}\right) \cdot \left(\frac{\rho_{\text{pi}}}{\rho_{\text{gel}}}\right) \cdot \left(\frac{\eta_{\text{gel}}}{\eta_{\text{pi}}}\right) \cdot (\text{time for pi to sag } 10\%)$$

where “pi” denotes “polyisoprene.” Plugging in the information in the statements of Problems 3.4(a) and 3.4(b), we obtain

$$1000\text{ hr} = \frac{1}{10} \cdot \frac{0.83}{3} \cdot \frac{\eta_{\text{gel}}}{8.46 \times 10^7\text{ P}} \cdot \frac{1}{6}\text{ hr}$$

From this we find

$$\eta_{\text{gel}} \approx 2 \times 10^{13}\text{ P}$$

Problem 3.5 Using the “universal hydrodynamic constant” $\Phi = 2.5 \times 10^{21}\text{ dL cm}^{-3}\text{ mol}^{-1}$ (where “dL” is deciliters), calculate the intrinsic viscosity for polyethylene of molecular weight $M = 10^6$ daltons. Note that for polyethylene, $C_\infty = 7.3$.

Problem 3.6 Derive Eq. (3-60) for the dumbbell model with a Warner spring.

Problem 3.7 Consider an entangled melt of linear flexible polymer chains of molecular weight $M = 100,000$ and zero-shear viscosity $\eta_0 = 10^4$ P. If M is increased to 300,000, what would η_0 be?

Problem 3.8 Numerically solve Eq. (3-78), the differential approximation to the Doi–Edwards equation for entangled linear melts, in a steady-state shearing flow. Plot the dimensionless shear stress σ_{12}/G against Weissenberg number $Wi \equiv \dot{\gamma}\tau$ for Wi between 0.1 and 100.

Problem 3.9 Integrate the Doi–Edwards equation (3-71) using the Currie expression for the \mathbf{Q} tensor, Eq. (3-75), for steady-state shearing, for $\dot{\gamma}\tau = 0.1, 0.3, 1.0, 3.0,$ and 10.0 , using only one relaxation time in the spectrum. Plot the values of dimensionless shear stress σ_{12}/G versus $\dot{\gamma}\tau$ on the same plot as in Problem 3.8. How close is the prediction of the approximate differential model to that of the “exact” integral model?

Problem 3.10 Suppose we approximate fast “Rouse” modes of entangled polymer molecules by a viscous stress, $\sigma^R \approx 2\eta^R\mathbf{D}$, with $\eta^R = 0.01G\tau$, and let the total shear stress $\sigma_{12}^{\text{total}} = \sigma_{12} + \sigma_{12}^R$, where σ_{12} is the stress computed in Problem 3.8. (See, for example, Fig. 3-33.) By plotting $\sigma_{12}^{\text{total}}/G$ against $\dot{\gamma}\tau$, estimate the values of $(\dot{\gamma}\tau)_{\text{max}}$ and $(\dot{\gamma}\tau)_{\text{min}}$ at which $\sigma_{12}^{\text{total}}$ has a relative maximum and a relative minimum. What will happen in a rheometer if one attempts to impose a shear rate $\dot{\gamma}$ with $(\dot{\gamma}\tau)_{\text{max}} < \dot{\gamma}\tau < (\dot{\gamma}\tau)_{\text{min}}$?

Problem 3.11 A theory incorporating “convective constraint release” and “chain stretch” into the Doi–Edwards model gives the constitutive equations below (Larson et al. 1998):

$$\frac{1}{\tau} = \frac{1}{\lambda^2\tau_d} + e^{-(\lambda-1)} \left(\mathbf{D} : \mathbf{S} - \frac{\dot{\lambda}}{\lambda} \right) \quad (\text{A3-29a})$$

$$\mathbf{S} = \int_{-\infty}^t \frac{1}{\tau(t')} \exp \left[- \int_{t'}^t \frac{dt''}{\tau(t'')} \right] \hat{\mathbf{Q}} dt' \quad (\text{A3-29b})$$

$$\dot{\lambda} = \lambda \mathbf{D} : \mathbf{S} - \frac{1}{\tau_r} (\lambda - 1) - \frac{1}{2} \left(\mathbf{D} : \mathbf{S} - \frac{\dot{\lambda}}{\lambda} \right) (\lambda - 1) \quad (\text{A3-29c})$$

$$\boldsymbol{\sigma} = 5G_N^0 \lambda^2 \mathbf{S} \quad (\text{A3-29d})$$

In the above, λ is the “chain stretch,” which is greater than unity when the flow is fast enough (i.e., $\dot{\gamma}\tau_r > 1$) that the retraction process is not complete, and the chain’s “primitive path” therefore becomes stretched. This magnifies the stress, as shown by the multiplier λ^2 in the equation for the stress tensor $\boldsymbol{\sigma}$, Eq. (3-78d). The tensor $\hat{\mathbf{Q}}$ is defined as $\hat{\mathbf{Q}} = \mathbf{Q}/5$, where \mathbf{Q} is defined by Eq. (3-70). Convective constraint release is responsible for the last terms in Eqns. (A3-29a) and (A3-29c); these cause the orientation relaxation time τ to be shorter than the reptation time τ_d and reduce the chain stretch λ . Derive the predicted dependence of the dimensionless shear stress σ_{12}/G_N^0 and the first normal stress difference N_1/G_N^0 on the dimensionless shear rate $\dot{\gamma}\tau_r$ for $\tau_d/\tau_r = 50$ and compare your results with those plotted in Fig. 3-35.

Problem 3.12 Suppose you have monodispersed star-branched melts of some polymer with molecular weights 20,000, 40,000, and 100,000. You measure the longest relaxation times of the two lower-molecular-weight samples and find $\tau_1 = 1$ sec and 10 sec, respectively, for $M =$

20,000 and $M = 40,000$. Estimate τ_1 for $M = 100,000$. From these results and Eq. (3-79), estimate M_e , the entanglement molecular weight.

Problem 3.13(a) (Worked Example) You have a “binary blend” containing two different molecular weights, M_L and M_S , of the same polymer. Let the weight fraction of M_L be ϕ , where M_L corresponds to the high molecular weight. Approximate the linear relaxation moduli of the pure melts by $G_L(t) = G_0 \exp(-t/\tau_L)$ and $G_S(t) = G_0 \exp(-t/\tau_S)$. Derive an expression for $G(t)$ for the blend from “double reptation” theory.

ANSWER:

For a molecular weight distribution with only two components, the integral in Eq. (3-78) is replaced by a sum:

$$\left(\frac{G(t)}{G_0}\right)^{1/2} = \phi \exp\left(\frac{-t}{2\tau_L}\right) + (1 - \phi) \exp\left(\frac{-t}{2\tau_S}\right)$$

Thus,

$$G(t) = G_0 \left[\phi \exp\left(\frac{-t}{2\tau_L}\right) + (1 - \phi) \exp\left(\frac{-t}{2\tau_S}\right) \right]^2 \quad (\text{A3-30})$$

Problem 3.13(b) (Worked Example) If $\tau_L \gg \tau_S$, then $G(t)$ of the blend has two plateaus, the second one corresponding to relaxation of the long molecules. The magnitude of the first plateau is obtained by taking the limit $t \ll \tau_S$, and the second plateau is obtained in the limit $t \gg \tau_S$, but $t < \tau_L$. Compute the modulus on the first and second plateaus. How does the second plateau modulus depend on ϕ ?

ANSWER:

Putting $t \ll \tau_S$ into Eq. (A3-30), both exponentials become unity; thus

$$G(t) = G_0[\phi + (1 - \phi)]^2 = G_0$$

So the first plateau is G_0 . For the second plateau, $t \gg \tau_S$, but $t < \tau_L$. Hence, the exponential $\exp(-t/\tau_S)$ is nearly zero. Thus, from Eq. (A3-30) we obtain

$$G(t) = G_0 \left[\phi \exp\left(\frac{-t}{2\tau_L}\right) \right]^2 = G_0 \phi^2 \exp\left(\frac{-t}{\tau_L}\right)$$

Thus, the modulus on the second plateau is $\phi^2 G_0$.

Problem 3.14 (Worked Example) Derive expressions for the shear viscosity and first and second normal stress coefficients in steady-state shearing of the Johnson–Segalman model, given by Eqs. (3-80) and (3-81a).

ANSWER:

From Eqs. (3-80) and (3-81a), the Johnson–Segalman model is

$$\overset{\nabla}{\sigma} + \frac{1}{\tau} \sigma + \xi(\mathbf{D} \cdot \sigma + \sigma \cdot \mathbf{D}) = 2G\mathbf{D} \quad (\text{A3-31})$$

At steady state, the upper-convected derivative, defined by Eq. (3-33), reduces to

$$\dot{\bar{\sigma}} = -\nabla \mathbf{v}^T \cdot \boldsymbol{\sigma} - \boldsymbol{\sigma} \cdot \nabla \mathbf{v} \quad (\text{A3-32})$$

For a simple shearing flow, we shall work in two dimensions, where “1” is the flow direction and “2” the gradient direction. The stress components σ_{i3} and σ_{3i} are zero, where $i = 1, 2$, or 3. The velocity gradient tensor is given by Eq. (1-6):

$$\nabla \mathbf{v} = \dot{\gamma} \begin{pmatrix} 0 & 0 \\ 1 & 0 \end{pmatrix}, \quad \nabla \mathbf{v}^T = \dot{\gamma} \begin{pmatrix} 0 & 1 \\ 0 & 0 \end{pmatrix} \quad (\text{A3-33})$$

Then, from Eq. (A3-32), we obtain

$$\dot{\bar{\sigma}} = -\dot{\gamma} \begin{pmatrix} 0 & 1 \\ 0 & 0 \end{pmatrix} \cdot \begin{pmatrix} \sigma_{11} & \sigma_{12} \\ \sigma_{12} & \sigma_{22} \end{pmatrix} - \dot{\gamma} \begin{pmatrix} \sigma_{11} & \sigma_{12} \\ \sigma_{12} & \sigma_{22} \end{pmatrix} \cdot \begin{pmatrix} 0 & 0 \\ 1 & 0 \end{pmatrix} = -\dot{\gamma} \begin{pmatrix} 2\sigma_{12} & \sigma_{22} \\ \sigma_{22} & 0 \end{pmatrix} \quad (\text{A3-34})$$

We note that

$$\mathbf{D} = \frac{1}{2} \dot{\gamma} (\nabla \mathbf{v} + \nabla \mathbf{v}^T) = \frac{1}{2} \dot{\gamma} \begin{pmatrix} 0 & 1 \\ 1 & 0 \end{pmatrix}$$

Therefore,

$$\begin{aligned} \xi(\mathbf{D} \cdot \boldsymbol{\sigma} + \boldsymbol{\sigma} \cdot \mathbf{D}) &= \frac{1}{2} \xi \dot{\gamma} \left\{ \begin{pmatrix} 0 & 1 \\ 1 & 0 \end{pmatrix} \cdot \begin{pmatrix} \sigma_{11} & \sigma_{12} \\ \sigma_{12} & \sigma_{22} \end{pmatrix} + \begin{pmatrix} \sigma_{11} & \sigma_{12} \\ \sigma_{12} & \sigma_{22} \end{pmatrix} \cdot \begin{pmatrix} 0 & 1 \\ 1 & 0 \end{pmatrix} \right\} \\ &= \xi \dot{\gamma} \begin{pmatrix} \sigma_{12} & 1/2(\sigma_{11} + \sigma_{22}) \\ 1/2(\sigma_{11} + \sigma_{22}) & \sigma_{12} \end{pmatrix} \end{aligned} \quad (\text{A3-35})$$

Using Eqs. (A3-34) and (A3-35), we can express Eq. (A3-31) as a set of component equations:

$$\text{11 Equation:} \quad -2\dot{\gamma}\sigma_{12} + \frac{1}{\tau}\sigma_{11} + \xi\dot{\gamma}\sigma_{12} = 0 \quad (\text{A3-36})$$

$$\text{22 Equation:} \quad 0 + \frac{1}{\tau}\sigma_{22} + \xi\dot{\gamma}\sigma_{12} = 0 \quad (\text{A3-37})$$

$$\text{12 Equation:} \quad -\dot{\gamma}\sigma_{22} + \frac{1}{\tau}\sigma_{12} + \frac{1}{2}\xi\dot{\gamma}(\sigma_{11} + \sigma_{22}) = G\dot{\gamma} \quad (\text{A3-38})$$

Solving Eq. (A3-36) for σ_{12} gives

$$\sigma_{12} = \frac{\sigma_{11}}{(2 - \xi)\dot{\gamma}\tau} \quad (\text{A3-39})$$

Likewise, we solve Eq. (A3-37), and use (A3-39) to replace σ_{12} :

$$\sigma_{22} = -\xi\dot{\gamma}\tau\sigma_{12} = -\xi\dot{\gamma}\tau \left(\frac{\sigma_{11}}{(2 - \xi)\dot{\gamma}\tau} \right) = -\frac{\xi}{2 - \xi}\sigma_{11} \quad (\text{A3-40})$$

We now use Eq. (A3-39) and (A3-40) to replace σ_{12} and σ_{22} in Eq. (A3-38), giving

$$\frac{\xi\dot{\gamma}\sigma_{11}}{2 - \xi} + \frac{1}{2}\xi\dot{\gamma} \left(\sigma_{11} - \frac{\xi\sigma_{11}}{2 - \xi} \right) + \frac{1}{\tau} \frac{\sigma_{11}}{(2 - \xi)\dot{\gamma}\tau} = G\dot{\gamma} \quad (\text{A3-41})$$

This equation can now be solved algebraically for σ_{11} , and the result can be used in Eq. (A3-39) and (A3-40) to obtain σ_{12} and σ_{22} . The results are

$$\sigma_{11} = \frac{(2 - \xi)G\dot{\gamma}^2\tau^2}{1 + (2\xi - \xi^2)\dot{\gamma}^2\tau^2} \quad (\text{A3-42})$$

$$\sigma_{22} = \frac{-\xi G \dot{\gamma}^2 \tau^2}{1 + (2\xi - \xi^2) \dot{\gamma}^2 \tau^2} \quad (\text{A3-43})$$

$$\sigma_{12} = \frac{G \dot{\gamma} \tau}{1 + (2\xi - \xi^2) \dot{\gamma}^2 \tau^2} \quad (\text{A3-44})$$

We use the definitions of the shear viscosity η , first normal stress coefficient Ψ_1 , and second normal stress coefficient Ψ_2 [from Eq. (1-24)] to obtain

$$\eta \equiv \frac{\sigma_{12}}{\dot{\gamma}} = \frac{G\tau}{1 + (2\xi - \xi^2) \dot{\gamma}^2 \tau^2}$$

$$\Psi_1 \equiv \frac{\sigma_{11} - \sigma_{22}}{\dot{\gamma}^2} = \frac{2G\tau^2}{1 + (2\xi - \xi^2) \dot{\gamma}^2 \tau^2}$$

$$\Psi_2 \equiv \frac{\sigma_{22} - \sigma_{33}}{\dot{\gamma}^2} = \frac{-\xi G\tau^2}{1 + (2\xi - \xi^2) \dot{\gamma}^2 \tau^2}$$

To obtain this last result, remember that $\sigma_{33} = 0$. The interested reader should plot these functions and ponder how realistic they are.

Problem 3.15 Consider a K-BKZ integral equation in a shearing flow with the form shown below:

$$\boldsymbol{\sigma} = \int_{-\infty}^t m(t-t') h(\gamma) \mathbf{C}^{-1} dt' \quad (\text{A3-45})$$

Suppose there is a single relaxation time, so that $m(t-t') = (G/\tau) \exp[-(t-t')]$, and suppose that $h(\gamma) = \exp(-\gamma)$. Calculate a formula for the steady-state shear viscosity as a function of shear rate. At high shear rate, what is the shear-thinning power-exponent p , with $\eta \propto \dot{\gamma}^{-p}$?

■